2018-01-01

Geant4 Study Of Protons - Body Interactions

Omar Hernandez Rodriguez
University of Texas at El Paso, ohernandez21@miners.utep.edu

GEANT4 STUDY OF PROTONS – BODY INTERACTIONS

OMAR HERNANDEZ RODRIGUEZ

Master's Program in Physics

APPROVED:

Jorge A. López, Ph.D., Chair

Marian Manciu, Ph.D.

Wei Qian, Ph.D.

Charles Ambler, Ph.D.
Dean of the Graduate School

DEDICATION

I dedicate this writing to my parents, brothers, and to my love by all the support along my studies.

GEANT4 STUDY OF PROTONS – TISSUE INTERACTIONS

by

OMAR HERNANDEZ RODRIGUEZ, B.S.

THESIS

Presented to the Faculty of the Graduate School of

The University of Texas at El Paso

in Partial Fulfillment

of the Requirements

for the Degree of

MASTER OF SCIENCE

Department of Physics

THE UNIVERSITY OF TEXAS AT EL PASO

May 2018

ACKNOWLEDGEMENTS

The work described in this thesis would not have been possible without the direct participation of Ph.D. candidate Jason Holmes from The Arizona State University, UTEP M.S. student Selim Romero, and my mentor Dr. Jorge A. López Gallardo.

I thank Physics Department of UTEP for supporting me with a teaching Assistantship, and with the travel expenses to present my work at the 2017 meeting of the Texas Section of the American Physical Society in Dallas, Texas.

Finally, I also thank the members of my thesis committee, Dr. Marian Manciu and Dr. Wei Qian, for their careful reading of this thesis, and all of my professors and the staff of the Physics Department for their continuous support during these two years.

ABSTRACT

Proton beam therapy for cancer treatment uses high-energy protons to destroy cancer cells, a problem that needs immediate attention is the determination of where in the body the protons are hitting, in real time, i.e. during the irradiation. One possibility is to pay attention to the gamma rays produced during the irradiation, and use the information they carry to infer the body part that produced the gamma ray.

This thesis presents the results of an investigation of the interaction of protons with different body parts. Focusing on gamma ray-producing interactions, the goal is to determine the type of interaction that produced the gamma rays. More explicitly, the study uses computer simulations of interactions of proton-tissue, proton-brain, proton-bone, etc., all of which produce gamma rays, to determine the characteristics of the gamma rays produced. If sufficiently different, such gamma ray signatures could be used to design gamma ray detectors that can be used to infer the source of gamma rays during irradiations.

The study uses CERN's GEANT4 particle interaction package to simulate the proton interactions with different body materials, and uses CERN's ROOT statistical package to analyze the data. In particular, the distribution of gamma ray energies, their full-width half-maximum, energy resolution, maximum height, and total number of counts are used as characterizing signatures. Based on these features, the study concludes that it is possible to use the gamma ray spectra to determine what type of interaction produced it.

TABLE OF CONTENTS

LIST OF TABLES

LIST OF FIGURES

CHAPTER 1: INTRODUCTION

Medicine and health care nowadays benefit from the application of nuclear and atomic physics for diagnostics and treatment of cancer. One of the newer treatments in radiation oncology physics is proton therapy which uses a beam of protons to irradiate diseased tissue. Proton therapy uses an accelerator to target tumors with a beam of high-energy protons to damage the cell's DNA and kill them. An advantage of proton therapy over other types of treatments (such as electron beam therapy, for instance), is the ability of the protons to deposit their energy in a narrow range minimizing irradiation to other parts of the body.

R.R. Wilson began experimenting with proton therapy in 1946 at the Harvard Cyclotron Laboratory [Wilson, 1946], but the technique further developed in 1954 at the Berkeley Radiation Laboratory in 1954, and fully implemented in hospitals in 1989 at the Clatterbridge Centre for Oncology [PTCOG, 2013], and in many hospitals worldwide afterwards.

In Figure 1.1 points the location of the proton therapy centers in the USA, yellow stars are the centers in operation, white stars are under construction or in a development centers and finally the green one is an expanding center [NAPT, 2016]. To date there are thousands of proton-beam treatments carried out annually in the USA. The present project stems from a collaboration between Dr. Jorge A. Lopez's group with Dr. Ricardo Alarcon's group from the Arizona State University and the Mayo Clinic Cancer Center in Scottsdale, AZ [Mayo, 2018].

Figure 1.1 Proton therapy centers in USA in 2016 (picture from national association for proton therapy).

Proton beam therapy uses protons that are shot to cancerous cells to eliminate them. Protons are particles with positive charge and can be accelerated by electromagnetic means, usually by a synchrotron or cyclotron; Figure 1.2 shows the basic workings of a cyclotron. The proton source (F) introduces protons in the chamber, the electric field (E) pushes the proton toward the left chamber where a magnetic field (B) makes the proton move in a circle. When the proton reaches region with the electric field again, the switcher (C) changes the direction of the electric field to give the proton an acceleration thus increasing its velocity and its radius of gyration in the right chamber. The process is repeated until the proton's path reaches the maximum radius and exits to hit the target (A). Since high-energy protons penetrate deeper than low-energy ones, protons are accelerated up to the velocity required to reach the depth of the tumor in the body.

The protons travel to the target inside the patient's body interacting with the tissue and destroying cancerous cells. Due to the fact that protons have a definite range of interaction, the damage is limited to a specific range of depth and does not go beyond the tumor unlike photon beam therapy which goes farther into deep tissues and can damage healthy tissue.

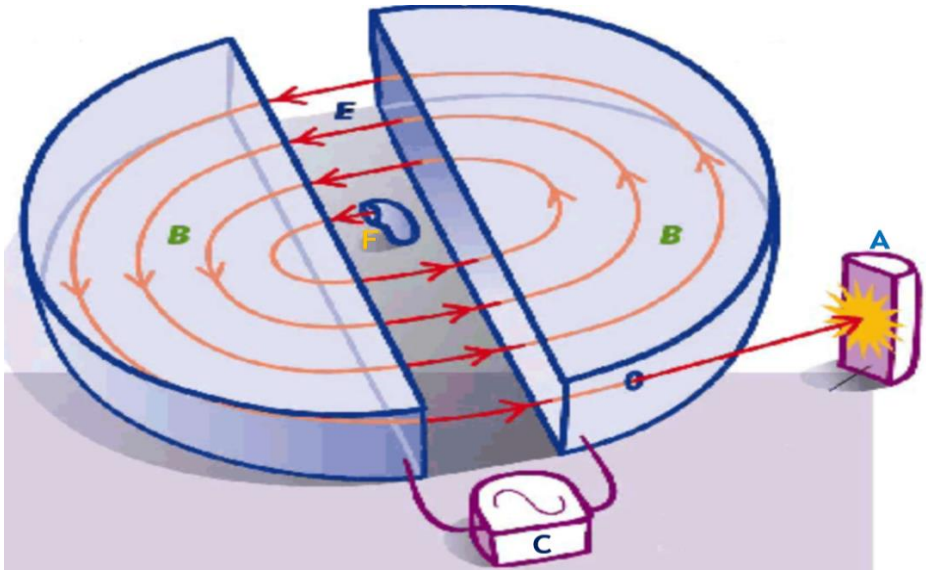

Figure 1.2 Simple understanding of a cyclotron.

Other benefits of proton therapy over other radiation treatments, is that it may deliver up 60% less radiation to healthy tissue around the tumor, it can also be applied in higher doses to the tumor causing less negative effects during and after treatment. As protons are more massive than electrons, for instance, they tend to have little lateral side scatter in the tissue keeping the beam narrow and focused on the tumor. As it will be explained in more detail in a future chapter, calibrating the proton energy allows the beam to deliver its energy in a certain range known as the Bragg peak [Camphausen, 2008]. Figure 1.3 shows a typical spread-out Bragg peak (SOBP) of an x-ray beam and a proton beam, the SOBP of the proton beam is actually produced by twelve Bragg peaks (blue lines) at different energies [Levin, 2005].

Proton beams used have energies in the range of 70 to 250 MeV where the energy is adjusted to focus the Bragg peak within the tumor, reducing radiation to healthy tissue closer to the surface of the body and a very small dose to tissue beyond the Bragg peak [Metz, 2006].

Depending of the depths of the tumor protons of different energies are used to add Bragg peaks at different depths to treat an entire tumor.

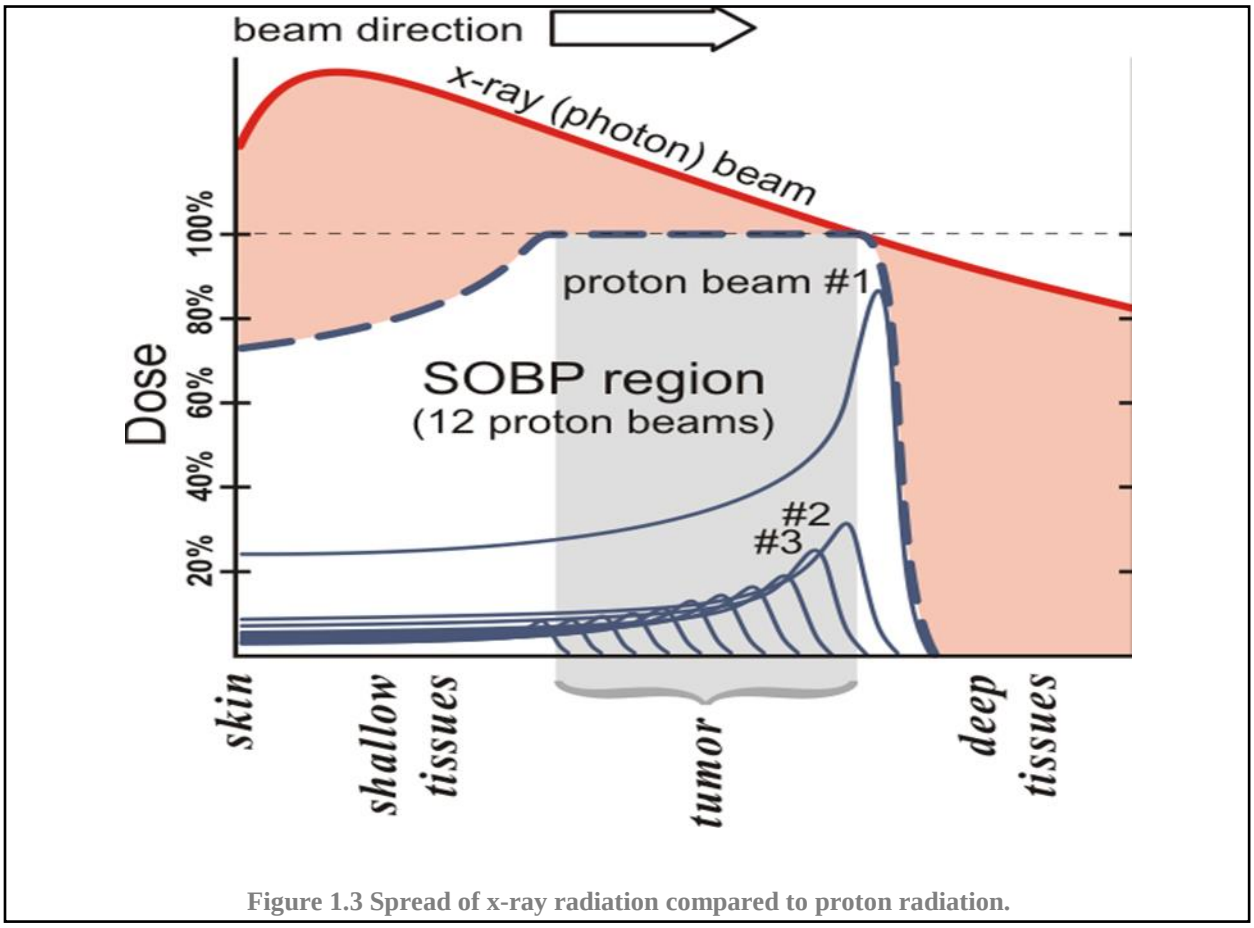

Figure 1.3 Spread of x-ray radiation compared to proton radiation.

Perhaps the most important question of proton therapy is, where exactly is the proton interacting? As the proton-cells interactions are invisible, it is impossible to know if the beam is actually damaging cancerous cells or healthy tissue. If information about the location of the target being hit by the proton beam were available (i.e. the SOBP), one could then fine-tune the beam energy during the irradiation for a better focus. Although indirect, it is possible to use the gamma rays produced during the proton-target interaction to determine the type of target being hit. This is the ultimate goal of this thesis, namely, to determine the type of target being irradiated.

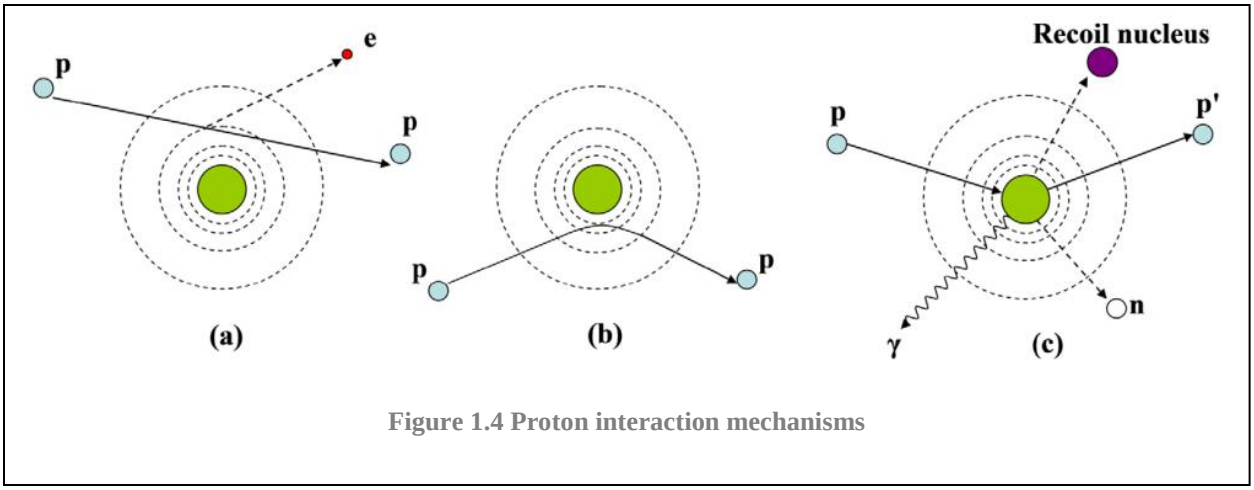

Figure 1.4 Proton interaction mechanisms

Figure 1.4. Proton interaction mechanisms: (a) proton-electron interactions, (b) deflection of proton by the nucleus Coulomb field, (c) proton-nucleus collision [Newhauser, 2015].

Protons interact with the tissue at the atomic level through the reactions shown in Figure 1.4. Out of those three types of reactions, only direct collisions of protons and nucleus lead to gamma ray production which can be detected outside the body during the irradiation. Although gamma rays can interact with matter in various ways (i.e. Mössbauer Effect, Coherent Scattering, Pair Production, Photoelectric Effect and Compton Effect [Nuclear Physics, 2017]), most of the time such interactions do not occur and the rays simply travel through the body freely in a straight line.

Moreover, the gamma ray producing proton-nucleus collisions are expected to be more or less intense depending on the density of the body being irradiated. As different body parts have varying densities (tissue being less dense that muscle, which is less dense than bone, etc.), the intensity of the gamma rays produced in different parts of the body is expected to vary, and thus could be used as a signal to identify the organ being irradiated. The specific goal of this thesis is to characterize the gamma rays produced by the different body parts when irradiated by a proton beam.

As it will be explained in detail later, the simulation package created by CERN Geant4 will be used to simulate the proton-body interactions, where body stands for bone, brain, tissue, etc. By varying the parameters of the simulation (beam energy, geometry, body part, etc.) thousands of simulations will produce gamma rays with varying energies and intensity. These characteristics of the gamma rays produced will be used as signatures to distinguish among the various targets.

In the next section we will discuss all the physics behind proton therapy such as the interaction of protons and how the gamma rays are created, etc. In Chapter 3 the program of Geant4 will be introduced along with a brief explanation of the program called ROOT that was used to process and plot all the data obtained from Geant4. In chapter 4 all the setup to perform all the simulation, such as body materials, energies, geometries etc., will be described. In Chapter 5 all the result of the simulations (gamma-ray spectra of different body materials) will be presented. Chapter 6 will present a series of conclusions extracted from this investigation.

CHAPTER 2: PHYSICS OF PROTON THERAPY

In this chapter the physics of proton-nucleus interactions will be described, as well as methods to characterize the gamma rays produced in such reactions.

2.1 PHYSICS OF PARTICLE-MATTER INTERACTIONS

In medical physics, the particles that intervene in therapies are the electrons, protons and neutrons, as well as x rays and gamma rays. Although nuclear reactions can be extremely complex, for medical physics purposes it suffices to take these particles as "ionizing radiation", for their ability to "ionize" (i.e. to remove electrons) from matter through which they propagate.

2.1.1 ELECTROMAGNETIC RADIATION

The term electromagnetic radiation here refers solely to x rays and gamma rays. The production of both of these rays is through the acceleration or deceleration of electric charges. "Soft" x rays carry energies in the range between 5 keV to 10 keV (or wavelength between 0.2 to 0.1 nm). "Hard" x rays have energies higher than 10 keV and up to 100 keV; these are useful in medical radiography because their wavelengths allow them to penetrate soft matter (tissue), at a difference of soft X-rays which are absorbed in air. Gamma rays carry energies higher than x rays; rays from radioactive decay have energies of up to 10 MeV.

X rays are produced by atomic means, i.e. when an electron jumps from a high energy level to a low energy in an atom producing an x ray photon; these X rays are known as K-shell or M-shell X rays. The most common means of production of x rays is by stopping an electron beam by a solid target (usually Mg, Al, etc.) which excites atomic electrons at a wide range of energies and producing X rays with a large number of wavelengths, such radiation is known as bremsstrahlung (braking radiation).

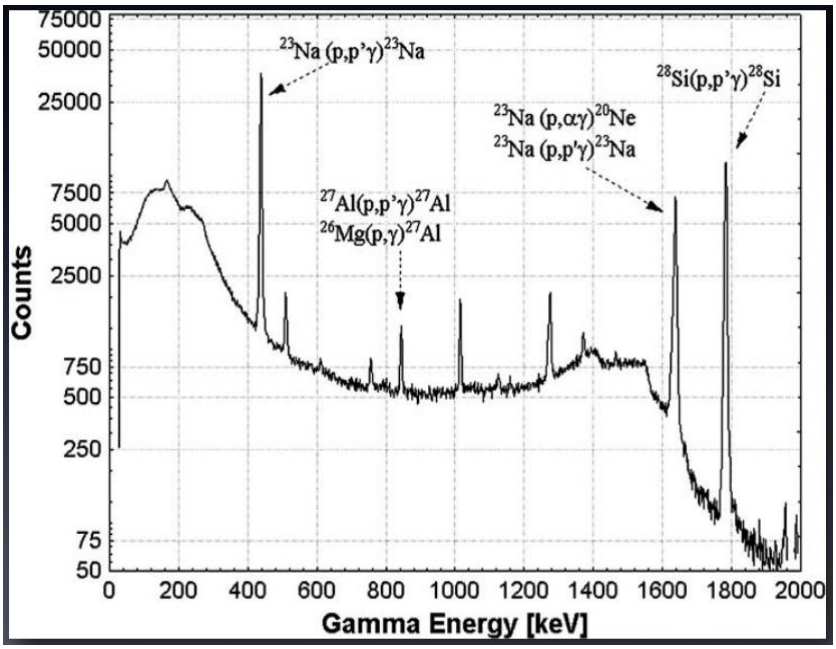

Figure 2.1. Characteristic gamma ray spectra in proton-induced reactions [chiari, 2013]. Clearly visible are the resonant peaks.

Gamma rays are produced by nuclear means, i.e. when nucleons (protons and neutrons) in a nucleus are excited by a passing charge (i.e. a proton in the proton beam) and de-excite by producing a gamma ray. Gamma rays have very small wavelengths (such as 10^{-11} m) and, thus, can travel through tissue as it were transparent.

2.1.2 PARTICLES AND INTERACTIONS

The most common interactions occurring between protons and atomic nuclei are presented in the Figure 1.4. Protons can interact with nuclei and produce gamma rays in several manners. Identifying nuclei as A, B, C, etc. excited nuclei as A*, B*, etc., protons as p, and gamma rays as γ, these interactions are:

A) Radiative capture: p + A → B* → B + γ, such as p + ^{27}Al → ^{28}Si + γ.

B) Inelastic scattering: p + A → A* → A + γ, such as p + ^{27}Al → p + ^{27}Al + γ.

C) Rearrangement collisions: p + A → C* → C + γ, such as p + ^{27}Al → ^{4}He + ^{24}Mg + γ.

Table 2.1 Prompt gamma energies (o).

Target	γ Energy (MeV)	Assignments
^{16}O	1.89	$^{16}O(p,pp\gamma_{1.89})\ ^{15}N$
	2	$^{16}O(p,x\gamma_{2.04})\ ^{15}O$
		$^{16}O(p,x\gamma_{2.00})\ ^{11}C$
	2.31	$^{16}O(p,x\gamma_{2.31})\ ^{14}N$
	2.8	$^{16}O(p,p'\gamma_{2.74})\ ^{16}O$
		$^{16}O(p,x\gamma_{2.79})\ ^{14}N$
		$^{16}O(p,x\gamma_{2.80})\ ^{11}C$
		$^{16}O(p,x\gamma_{2.87})\ ^{10}B$
	3.68	$^{16}O(p,x\gamma_{3.68})\ ^{13}C$
	4.44	$^{16}O(p,x\gamma_{4.44})\ ^{12}C$
	5.2	$^{16}O(p,x\gamma_{5.24})\ ^{15}O$
		$^{16}O(p,pp\gamma_{5.27})\ ^{15}N$
		$^{16}O(p,pp\gamma_{5.18})\ ^{15}O$
		$^{16}O(p,pp\gamma_{5.30})\ ^{15}N$
	6.1	$^{16}O(p,p'\gamma_{6.18})\ ^{16}O$
		$^{16}O(p,pp6.18)\ ^{15}O$

The gamma rays from these reactions are emitted with a wide range of energies. The proton-nucleus interaction is a quantum process in which the incident proton loses energy exciting the charges of the nucleus producing gamma rays in a process similar to x rays bremsstrahlung. At some energies, a resonant effect increases the yield of gammas; these energies are known as resonance energies (E_R) and the gamma yield peak is known as "Lewis Peak". Figure 2.1 shows a gamma ray spectrum produced in proton-nucleus reactions with the resonant peaks clearly visible. Table 2.1 lists the energies of gammas produced in proton irradiation of a ^{16}O target.

Due to its very short wavelength, gamma rays are the most penetrating radiation known. Gamma rays are known to penetrate easily body tissue, and it can only be stopped by a few centimeters of lead or about 1 meter of concrete. Although gamma rays can ionize atoms they encounter in their path, most gamma rays will simply travel through the body without any interaction. Since tissue and bone are practically transparent to gamma rays, once produced inside a human body, the gammas will exit in straight lines, and thus it is feasible to use this type of radiation to determine the proton interaction that produced the gammas.

2.1.3 PROTON THERAPY PHYSICS

The stopping power of a medium is proportional to the rate of energy loss according to:

$$S(E) = \frac{1}{\rho}\frac{\partial E}{\partial z}. \tag{2.1}$$

Where ρ is the density of the medium, $S(E)$ is the stopping power of charged particles with energy E, and z is the direction of motion, and for charged particles that have masses much larger than the electron mass m_e (such as the proton, $m_p \approx 2000\ m_e$), expression 2.1 becomes the Bethe equation:

$$S(E) = 0.307\frac{Z}{A}\left(\frac{1}{\beta^2}\right)\left(\frac{1}{2}\ln\frac{2m_e c^2\gamma^2\beta^2 T_{max}}{I^2} - \beta^2\right). \tag{2.2}$$

Where $= \frac{v}{c}$, $\gamma = \frac{1}{\sqrt{1-\beta^2}}$, T_{max} is the maximum transferable energy to an electron, I is the mean ionization potential of the media, A is the mass number, and Z the atomic number.

The stopping power of a material decreases as the beam speed v increases, i.e. $S(E)$ α $\frac{1}{v^2}$. This combination of the Bethe equation with a statistical Coulomb interaction leads the curves

shown in Figure 2.3 of the absorbed dose deposited by as a function of depth along the axis of the beam [Knopf, 2013]; the pronounced peak at a certain location is known as the Bragg peak. Figure 2.3 shows the great difference between the curve of photons and protons (cf. Figure 2.1). The area under each curve is proportional to the energy delivered indicates that different beams cause different amount of damage lengthwise along the trajectory of the beam. The advantage of protons over other types of beams in depositing energy in a specific region is clearly observable in Figure 2.3: by combining (pristine) beams at different energies it is possible to produce a spread-out Bragg peak (SOBP) that irradiates a larger but specific area, not damaging healthy tissue nearby.

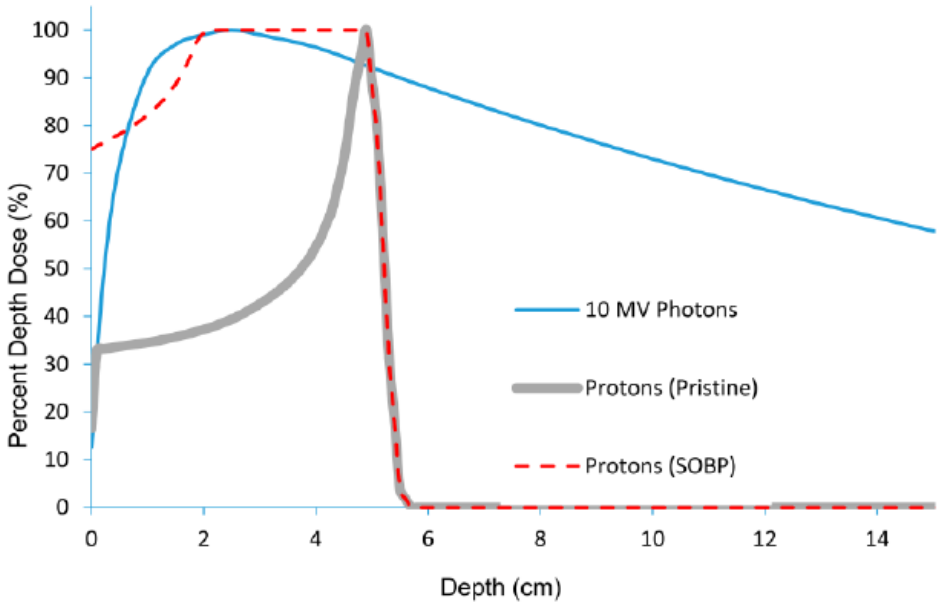

Figure 2.2. Percent depth dose as a function of depth [bernam, 2015].

2.2 THIS THESIS

There are two huge risks on radiotherapy, and it is the inherent uncertainty of the method. The first one, it is the uncertainty if the beam is depositing energy where is needed, and the second one, it is the possibility to damage any healthy tissue. Although these questions can be answered

by analyzing a biopsy, but using this method of biopsy, it is too late to prevent damage to healthy tissue or vital organ, it would be better to be able to answer them during the irradiation, i.e. *in vivo*; and this could be possible using gamma ray detectors during the application of the dose. The purpose of this thesis born from the needed of an accurate measurement of gamma ray detectors. In previous studies develop by Arizona State University (AST), this study will be a contribution to a new gamma ray detector that they have been being developing by AST for a student of PhD in physics Jason Holmes, this simulation in GEANT4 (GEometry ANd Tracking) will help in proton therapy because it has been studied the difference of gamma rays produced in proton-water interactions and proton-tissue interactions. Using Geant4 high energy protons are used to bombard different body materials at various energies and the gamma rays produced are compared to those produced in the case of proton-water collisions. The difference in gamma energy peaks between the water's histogram and the body materials will help us determine the gamma ray detector sensibility needed for the real-life scenario.

The focus of this thesis is to investigate the characteristics of the gammas produced in different types of proton interactions (e.g. proton-bone, proton-brain, etc.), and use such characteristics to identify in real time the type of interaction that takes place during an irradiation. For this purpose, Geant4 simulations will be used to generate data produced by the different types of reactions, and compare their respective energy spectra through a peak analysis, to determine if indeed it is possible to identify the target in a proton beam irradiation in real time during the irradiation.

CHAPTER 3: GEANT4

Geant4 is a computer platform to simulation the passage of particles through matter. It is used by particle physicists all over the world to study high energy reactions, nuclear physicists to study nuclear reactions, space engineers to study cosmic ray interactions with spacecrafts, and medical physicists to study the interaction of ionizing beams with the human body. Genat4 was designed to meet the demand for accurate simulations of particle detectors used at CERN. Geant4 is based on physics models developed from experimental results sampled according to Monte Carlo sampling, to handle the interactions between incident particles and matter for a wide energy range, from 250 eV to 1 TeV.

The program simply simulates the emission of specified particles at a given energy as a projectile, randomly choses an interaction with a given target, and tracks the products from the reaction. Through Monte Carlo methods the phenomena that rules the prescribed reactions is used to populate all of the possible outcomes allowed by the physical laws, producing robust statistics from which the reactions can be understood.

GEANT (for GEometry ANd Tracking) was first developed at the European Organization for Nuclear Research, CERN, but it was updated by many physicists from many countries [Nuclear Physics, 2015]. After years of improvement Geant4 was conceived in 1993 as an upgrade to the existing FORTRAN based Geant3 simulation program to construct an entirely new program based on object-oriented technology. The initiative became an international collaboration of physicist programmers and software engineers from Europe, Japan, Canada and the United States. Geant4 was released in 1998, and after several improvements it is the largest project of its kind outside the corporate world. [Geant4, 2018].

3.1 STRUCTURE OF GEANT4

Geant4 mimics aspects of a projectile-target interaction as well as all of the aspects of the detection of the reaction products. Geant4 allow the selection of:

- The geometry of the system,
- The materials involved,
- The generation of primary events,
- The tracking of particles through materials and electromagnetic fields,
- The physics processes governing particle interactions,
- The response of sensitive detector components,
- The generation of event data,
- The storage of events and tracks,
- The visualization of the detector and particles trajectories, and
- The capture and analysis of simulation data at different levels of detail and, refinement.

It is possible to construct stand-alone Geant4 applications using user interfaces, built-in steering routines, and command interpreters. Geant4 has a large set of physicals models to handle the interactions of particles with matter across a very wide energy range, indeed it contains a database with a large part of all that is known about particle interactions. Geant4 allows for the selection of energy ranges, particle types, target material and environment atmosphere.

Geant4 is written in C++ and the user must know C++ to be able to design an application. It uses advanced software-engineering techniques and object-oriented technology, most simulation options exist in the form of C++ structures and classes supplied by the toolkit. [Geant4, 2018].

3.2 OVERVIEW OF GEANT4 FUNCTIONALITY

The Geant4 class category diagram is shown in Figure 3.2. Categories at the bottom of the diagram are used by virtual all higher categories and provide the foundation of the toolkit.

- Global: category covers the system of units, constant, numeric and random number handling.
- Materials and particles: Implement facilities necessary describe the physical properties of particles and materials for the simulation of a particle -matter interactions.
- Geometry: above these reside categories required to describe the tracking of particles and the physical processes they undergo.

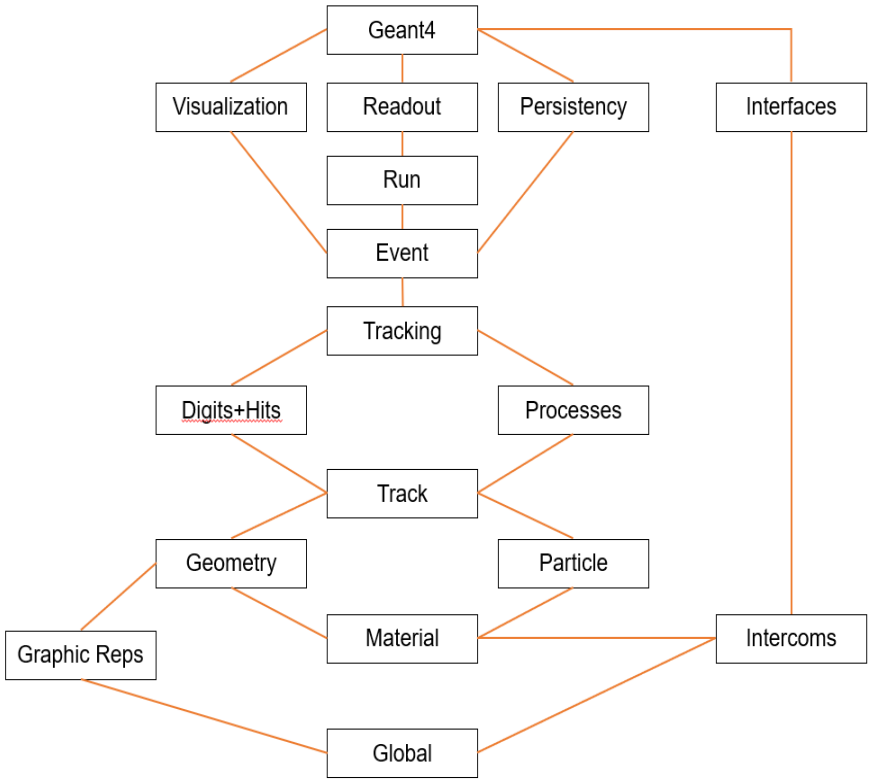

Figure 3.1 Geant4 class categories.

- Track: category contains classes for tracks and steps.
- Processes: category, which contains implementations of models of physical interactions: electromagnetic interactions of leptons, photons, hadrons and ions, and hadronic interactions.
- Tracking: category, which, manages their contribution to the evolution of track's state and pro vides information in sensitive volumes for hits and digitization.

Above these are:

- Event: category manages events in terms of their tracks
- Run: category manages collections of events that share a common beam and detector implementation.
- Readout: category allows the handling of pile-up.

Finally, capabilities that use all these categories and connect to facilities outside the toolkit through abstract interfaces, provide visualization, persistency, and user interface capabilities.

3.3 ROOT

ROOT is a framework for data processing created at CERN to analyze Geant4 data. From Geant4 the data can be saved along with any C++ object in a compressed binary form in ROOT files. ROOT provides a data structure tree which is extremely useful for fast access of huge amounts of data, orders of magnitude faster than accessing a normal file. Important features in ROOT, is its ability to represent results as histograms, scatter plots, fitting functions, etc. as well as the possibility to build personalized applications, use macros, use the Cling C++ interpreter for interactive sessions, or compile the program for faster running [ROOT, 2018].

CHAPTER 4: SIMULATIONS

The phenomenon we want t0o study is the generation of gammas in proton induced reactions. As a first step the simulation must contain a proton beam with certain proton energy and a given energy dispersion, as well as a given direction and a given dispersion. Next the simulation must contain a target at some location, along with the physics rules for the proton beam – target interaction. Such physical rules should include the generation of gamma rays through these reactions in a realistic manner so that the gammas are produced in the proper directions dictated by the reactions, and with the proper energies. As a final step the simulation should have a gamma ray detector to count the gammas produced, and quantify their direction and energies. More specifically, we will need to simulate a very large number of protons ($1x10^6$events) shooting over different body materials (lung, brain, blood, etc.) and at different energies.

4.1 DEFINITION OF GEOMETRY AND BODY MATERIALS

The main program of proton interactions with different body materials has subprograms such as Action Initialization, Detector Constructor, Event Action, Primary Generator, Run Action, etc. where the definitions of geometries and body materials are created.

```
// Geometry parameters

G4double worldSizeX = 50*cm;
G4double worldSizeY = 50*cm;
G4double worldSizeZ = 50*cm;
G4double targetSizeX = 20*cm;
G4double targetSizeY = 20*cm;
G4double targetSizeZ = 20*cm;
```

Figure 4.1 Geometry parameters.

The first step in this simulation is to create what is called the “world”, which is the total volume defined for the simulation (Figure 4.1); this world contains the proton beam, targets, particles produced in the reactions, detectors and all the space in between. Particles and radiation simply cannot exist outside the world, the data and interactions exist only inside this volume (Figure 4.2). A sub-volume of important is the one that contains the target and will receive the protons. A third sub-volume is that of the detector which in principle can mimic a real detector. In our case, as we are interested only in the number of gammas produced and not on the actual efficiency of a real detector, the gammas are simply counted as they are produced in the second sub-volume. As the body is, in large percentage made of water, the second sub-volume is filled with water and it is named “water phantom”; in our case the water phantom works both as container for different body materials as well as a counter (Figure 4.2).

```
// World
//
G4VSolid* worldS
  = new G4Box("World",           // its name
              worldSizeX/2, worldSizeY/2, worldSizeZ/2); // its size

G4LogicalVolume* worldLV
  = new G4LogicalVolume(
              worldS,           // its solid
              defaultMaterial,  // its material
              "World");         // its name

G4VPhysicalVolume* worldPV
  = new G4PVPlacement(
              0,                // no rotation
              G4ThreeVector(),  // at (0,0,0)
              worldLV,          // its logical volume
              "World",          // its name
              0,                // its mother  volume
              false,            // no boolean operation
              0,                // copy number
              fCheckOverlaps);  // checking overlaps

//
//  water  Phantom
//  G4Box
G4VSolid* targetBoxS
  = new G4Box("TargetBox",           // its name
              targetSizeX/2, targetSizeY/2, targetSizeZ/2); // its size

G4LogicalVolume* targetBoxLV
  = new G4LogicalVolume(
              targetBoxS,           // its solid
```

Figure 4.2 Definition of world and water phantom

Table 4.1 Some geant4 material database.

NIST Compounds		
==========	==========	==========
Ncomp	density(g/cm^3)	I(eV)
==========	==========	==========
6 G4_A-150_TISSUE	1.127	65.1
4 G4_AIR	0.00120479	85.7
6 G4_B-100_BONE	1.45	85.9
14 G4_BLOOD_ICRP	1.06	75.2
8 G4_BONE_COMPACT_ICRU	1.85	91.9
9 G4_BONE_CORTICAL_ICRP	1.85	106.4
13 G4_BRAIN_ICRP	1.03	73.3
4 G4_EYE_LENS_ICRP	1.1	73.3
13 G4_LUNG_ICRP	1.05	75.3
6 G4_MS20_TISSUE	1	75.1
13 G4_MUSCLE_SKELETAL_ICRP	1.04	75.3
9 G4_MUSCLE_STRIATED_ICRU	1.04	74.7
4 G4_MUSCLE_WITH_SUCROSE	1.11	74.3
4 G4_MUSCLE_WITHOUT_SUCROSE	1.07	74.2
13 G4_SKIN_ICRP	1.1	72.7
13 G4_TISSUE_SOFT_ICRP	1	72.3
4 G4_TISSUE_SOFT_ICRU-4	1	74.9
4 G4_TISSUE-METHANE	0.00106409	61.2
4 G4_TISSUE-PROPANE	0.00182628	59.5
2 G4_WATER H_2O	1	75

4.2 DEFINITION OF PARTICLES AND ENERGIES

Body materials are declared from Geant4 Material Database (Table 4.1). The proton-target interactions are defined is in the subprograms Action Initialization, Detector Constructor, Event

Action, Primary Generator, Run Action, Calorimeter, etc. (Figure 4.3), the declaration of particles (only protons in this case) and their interactions with the different body materials is done in the Calorimeter; the body parts in our case will be water, muscle, lung, brain, bone, blood, Muscle with and without sucrose, striated muscle, and skeletal muscle. Again, the reactions and data of interest are those involving only protons and gamma rays, all other possible reactions are not simulated as they do not produce gammas and are not of interest for our work.

```
// get the particle name
const G4String particleName = step->GetTrack()->GetDefinition()->GetParticleName();

if (strcmp(particleName,"proton") == 0 && edep == 0. && stepLength == 0. ) return false;

G4TouchableHistory* touchable
  = (G4TouchableHistory*)(step->GetPreStepPoint()->GetTouchable());

// Get calorimeter cell id
G4int layerNumber = touchable->GetReplicaNumber(1);

// Get hit accounting data for this cell
B4cCalorHit* hit = (*fHitsCollection)[layerNumber];
if ( ! hit ) {
  G4ExceptionDescription msg;
  msg << "Cannot access hit " << layerNumber;
  G4Exception("B4cCalorimeterSD::ProcessHits()",
    "MyCode0004", FatalException, msg);
}

// fill the histogram on a step by step basis

G4AnalysisManager* analysisManager = G4AnalysisManager::Instance();

if (strcmp(particleName,"proton") == 0) {
  analysisManager->FillH1(1, pos.getZ(), edep);
}
if (strcmp(particleName,"gamma") == 0 && kineticEnergy > 0.01*MeV) {
  analysisManager->FillH1(2, kineticEnergy);
  step->GetTrack()->SetTrackStatus(fStopAndKill);
}
```

Figure 4.3 Declaration of particles and histograms.

The beam energies are defined in the class “RunBeam”; in this work three energy values were used: 60 MeV, 80 MeV and 120 MeV. Figure 4.4 shows the declaration and initialization of the program, class of gun, in this case is a proton particle with energy of 120 MeV and 10,000,000 particles fired.

The simulations were computed in a personal computer with Intel i7 processors and each run lasted up to 20 minutes. Altogether close to one billion runs were simulated. The results are presented next.

```
/run/initialize
/tracking/verbose 0
/gun/particle proton
/gun/energy 120 MeV
/run/beamOn 10000000
```

Figure 4.4 Declaration of "runbeam".

CHAPTER 5: SIMULATIONS, RESULTS AND ANALYSIS

5.1 SIMULATIONS

As explained before, the simulations started with the creation of a "world", a proton beam, and a "water phantom" representing both the target and the counter. All of the simulations were performed with the same dimensions for the "world" and "water phantom", the only changes between the different cases were the target material (i.e. the body part used) in the water phantom. Figure 5.1 shows a typical graphic representation of a simulation with the world (large external cube), protons (blue lines) hitting the water phantom (inside cube), producing gamma rays (green lines) and electrons (red lines).

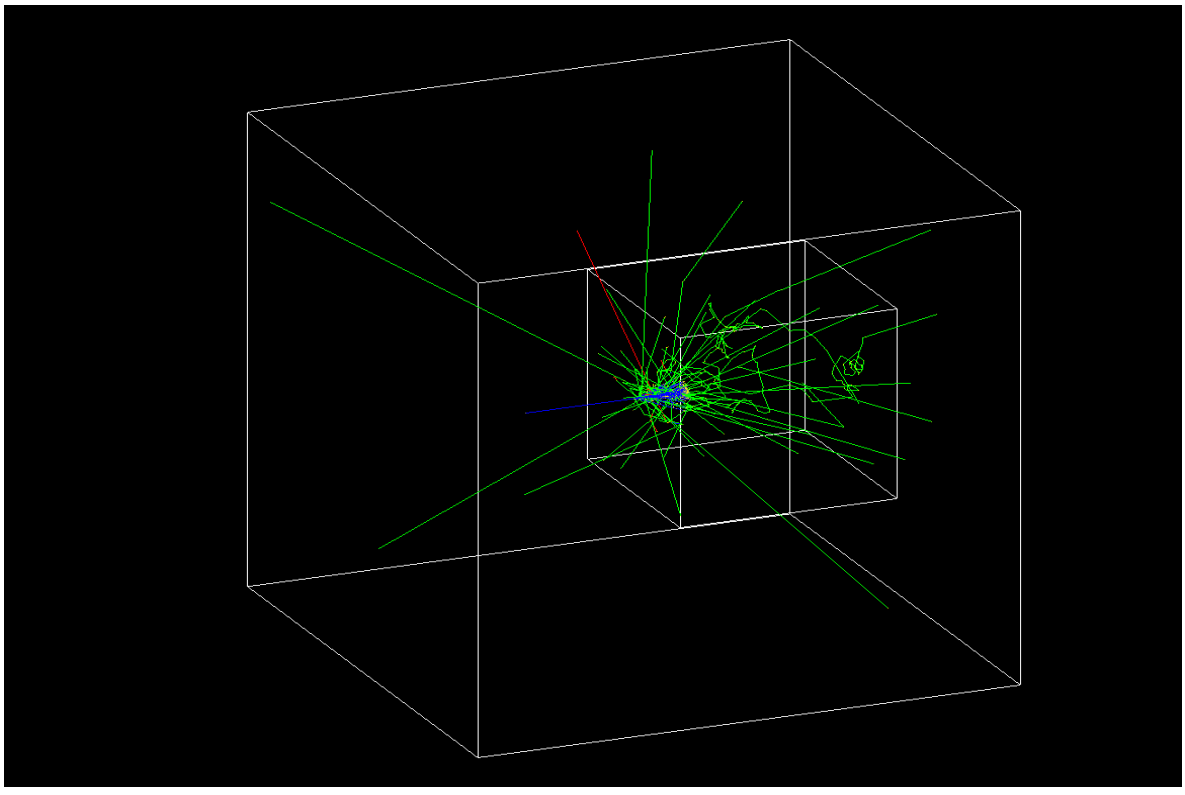

Figure 5.1 Geant4 simulation of protons hitting a cube of water.

Given that the SOBP needed is obtained with beam energies between 70 MeV and 210 MeV, we run preliminary simulations with three beam energies (60 MeV, 120 MeV and 180 MeV). Figure 5.2 shows the gamma ray spectra obtained with protons interacting with water at the three beam energies. The figure clearly shows several resonance peaks and illustrates the fact that the number of gamma rays will be higher for higher energies. Since the peak characteristic are very similar for all three energies, the rest of the simulations were performed with an energy of 120 MeV.

The beam was directed always in the same direction in all of the simulations. The gamma ray spectra were obtained in the energy range of 0 to 1000 MeV. The energies of the gamma ray produced were counted in bins of 0.2 MeV. All gammas were counted independent of their direction; this will aid in the future design of a real detector in a later part of the project. The gamma ray spectrum histograms have their vertical axis counting from 0 to 3000 gamma rays (i.e. the number of gamma rays produced in the water phantom), and with the horizontal axis representing the energy of each gamma ray bin running from 1.5 to 6.5 MeV were the resonant peaks of interest exist.

5.2 RESULTS

The histograms were obtained with CERN's ROOT which is the scientific software framework used for big data processing, statistical analysis, visualization, and storage. Further analysis includes a Gaussian fit of each of the resonance peaks, the integration of the peaks, determination of the full width half maximum, the maximum number of counts, and the peak resolution (to be defined next). Figure 5.3 shows the programming used in ROOT to determine the integrations of each of the resonant peaks.

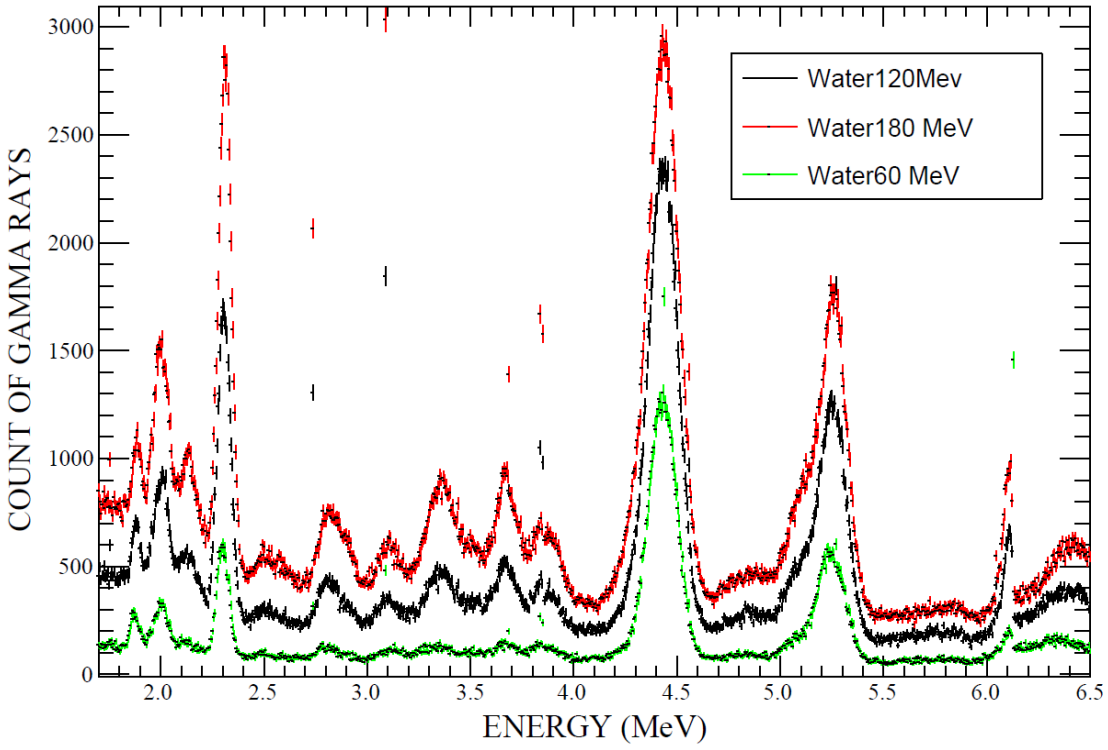

Figure 5.2 Energy spectra of proton-induced prompt gamma-rays in water.

```
void simAnalysis(char* fileName) {

  TFile* resultsFile = new TFile(fileName);

  TH1D* histo1 = (TH1D*)resultsFile->Get("1");
  TH1D* histo2 = (TH1D*)resultsFile->Get("2");

  int numBins = histo1->GetNbinsX();

  double integralTotal = histo2->Integral();
  double integraltotalrevision = histo2->Integral(0, 1000);
  double integral1 = histo2->Integral(185,215);
  double integral2 = histo2->Integral(215,245);
  double integral3 = histo2->Integral(265,295);
  double integral4 = histo2->Integral(355,375);
  double integral5 = histo2->Integral(420,460);
  double integral6 = histo2->Integral(505,535);
  double integral7 = histo2->Integral(595,625);
```

Figure 5.3 Range of peak's integrations.

The following figures show the histograms obtained by irradiating protons on water (Figure 5.4), muscle tissue (Figure 5.5), lung tissue (Figure 5.6), brain tissue (Figure 5.7), bone (Figure 5.8), blood (Figure 5.9), tissue (Figure 5.10), Muscle with sucrose (Figure 5.11), Muscle without sucrose (Figure 5.12), striated muscle (Figure 5.13), and skeletal muscle (Figure 5.14). Comparison among the different spectra will help us to identify differences that can be used to determine the target producing gamma rays in real irradiations.

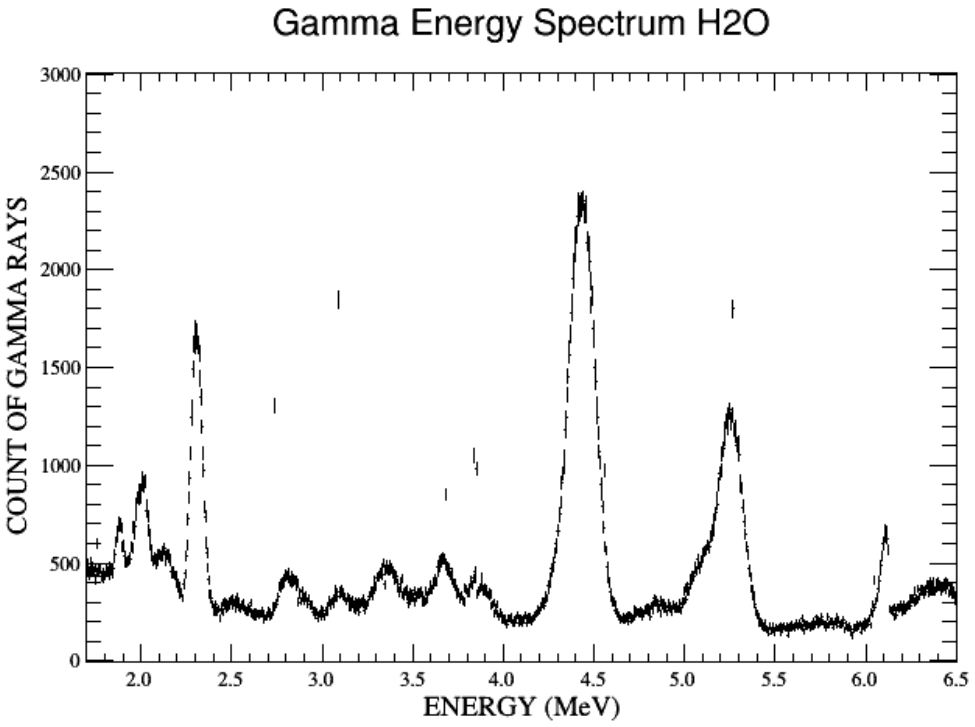

Figure 5.4 Gamma energy spectrum water.

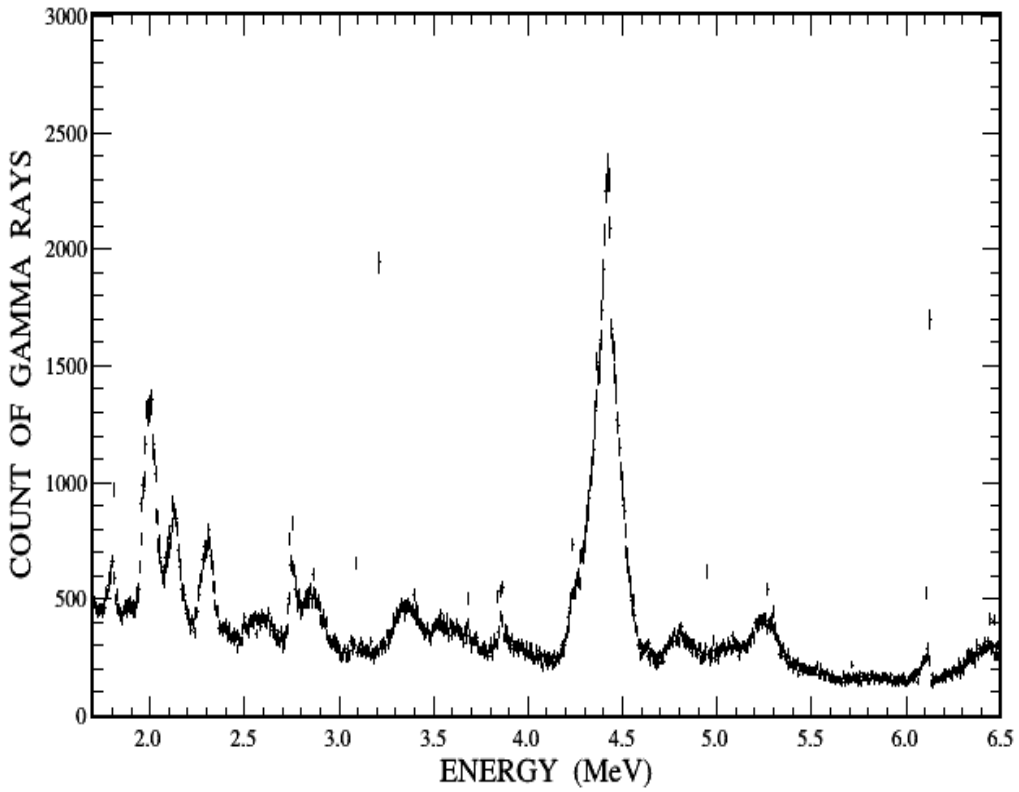

Figure 5.5 Gamma energy spectrum ms20-tissue.

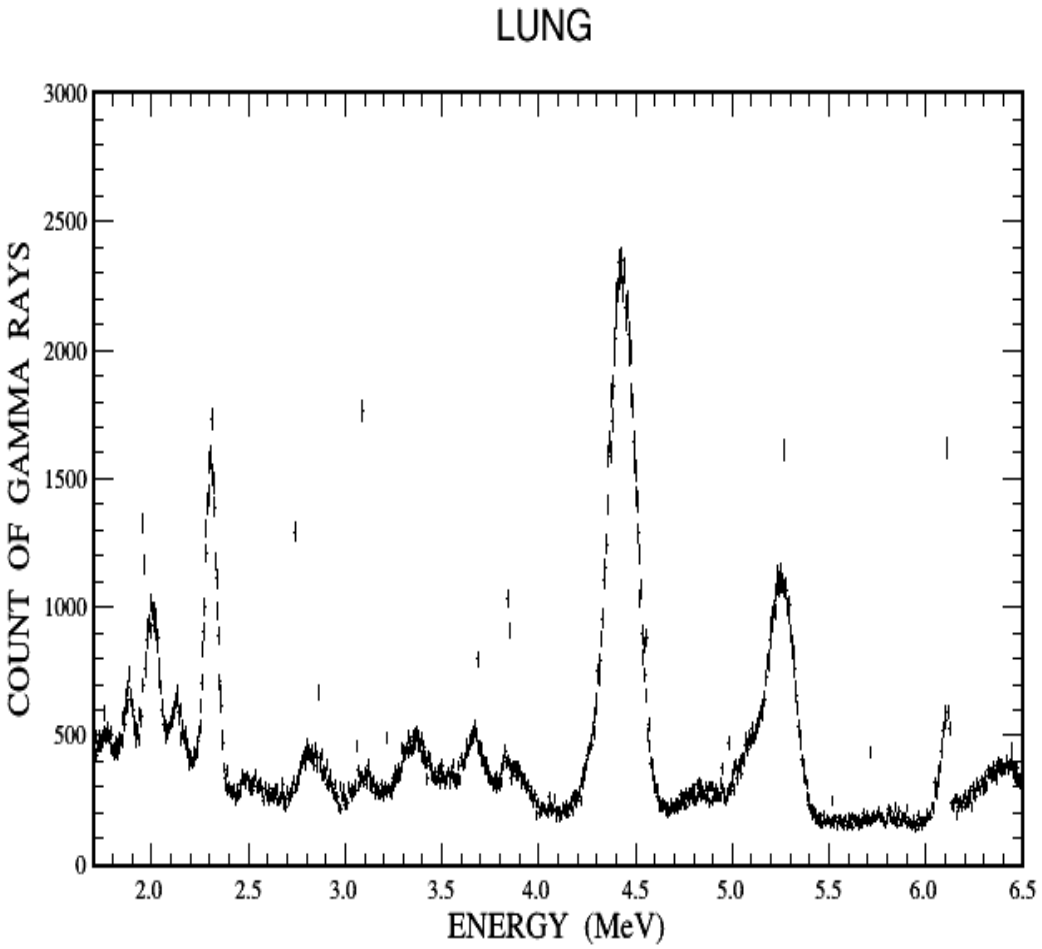

Figure 5.6 Gamma energy spectrum lung.

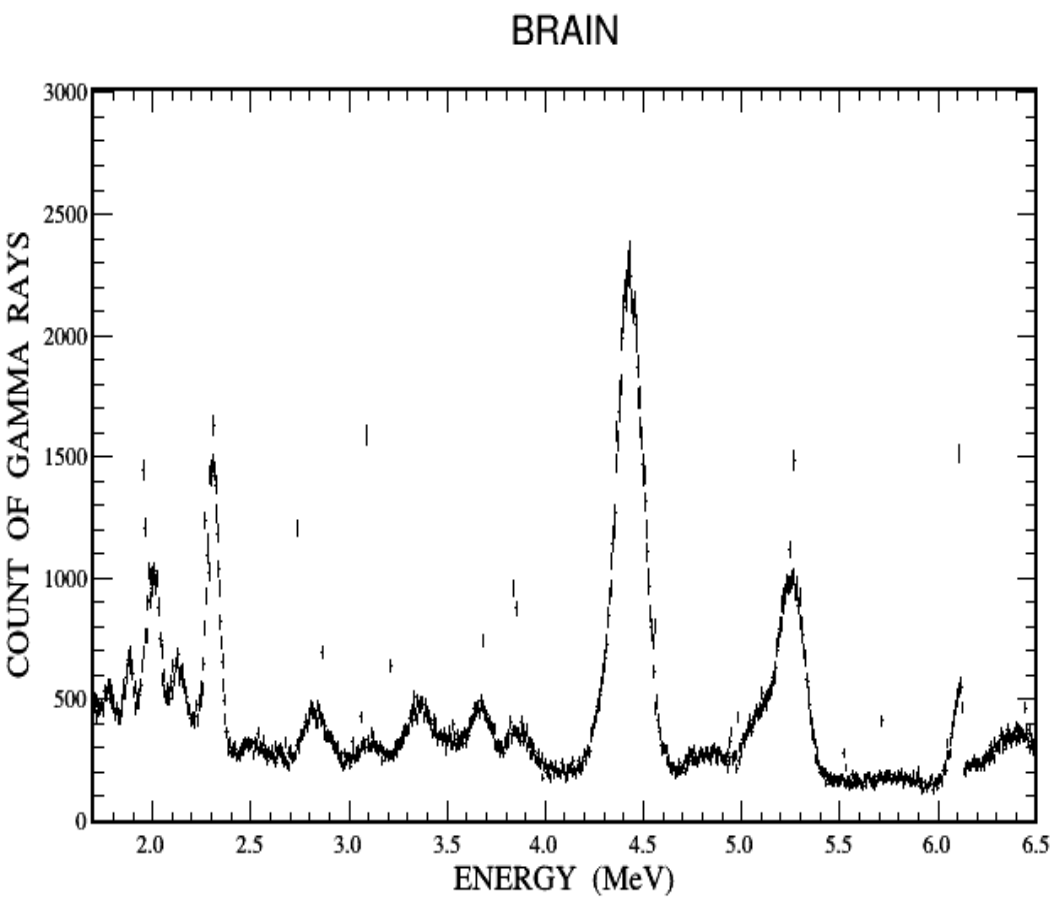

Figure 5.7 Gamma energy spectrum brain.

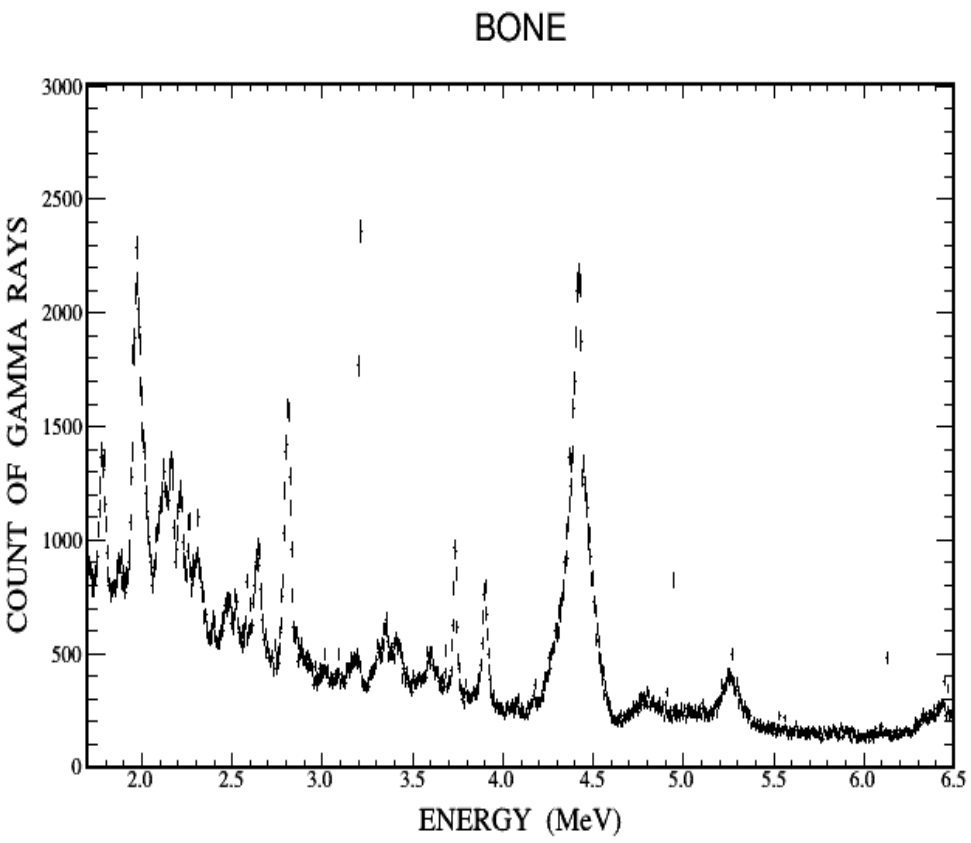

Figure 5.8 Gamma energy spectrum bone.

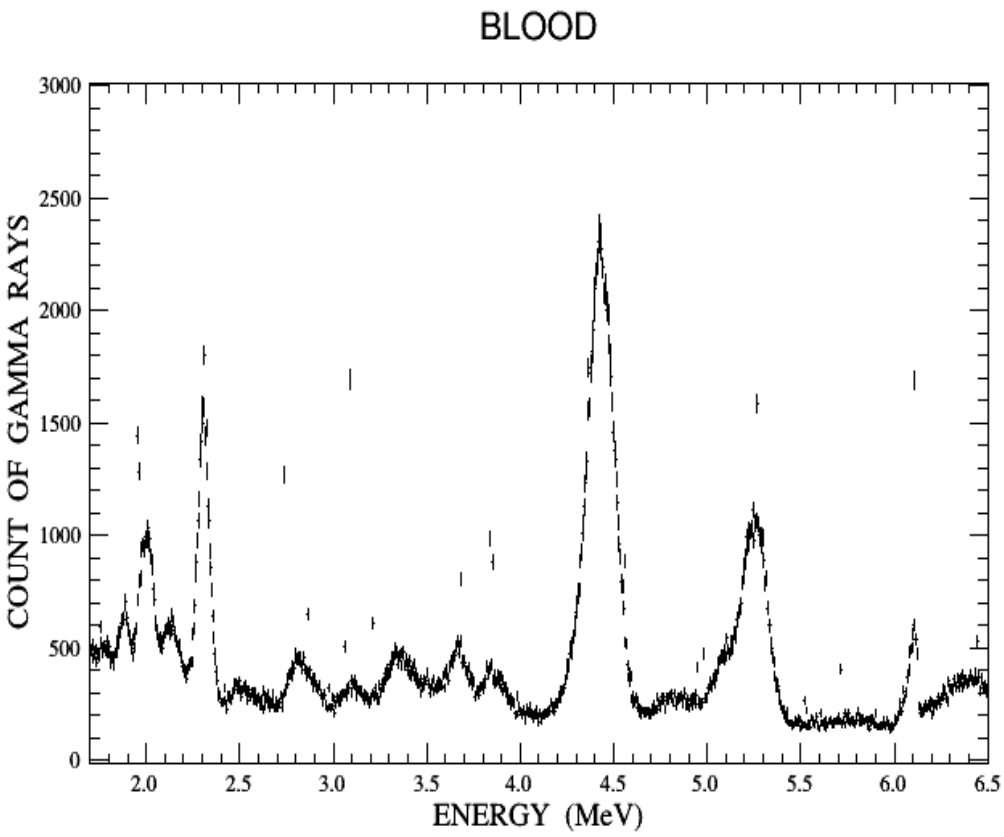

Figure 5.9 Gamma energy spectrum blood.

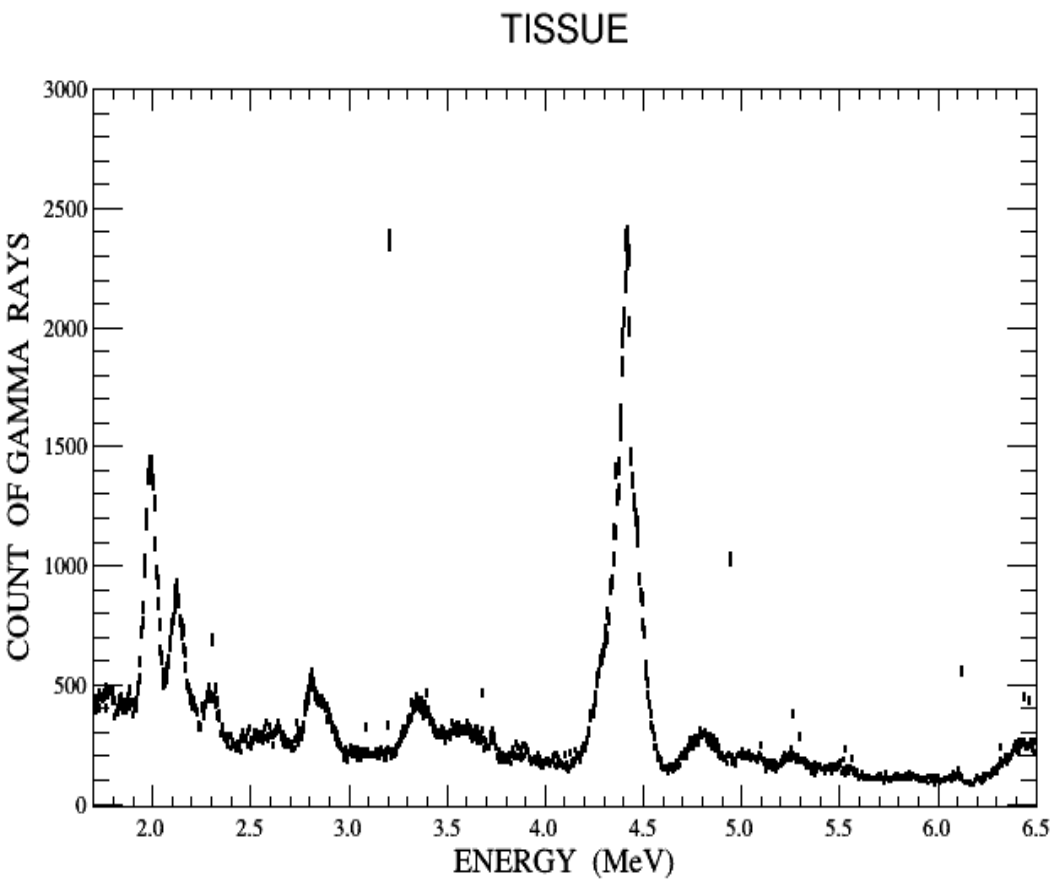

Figure 5.10 Gamma energy spectrum tissue.

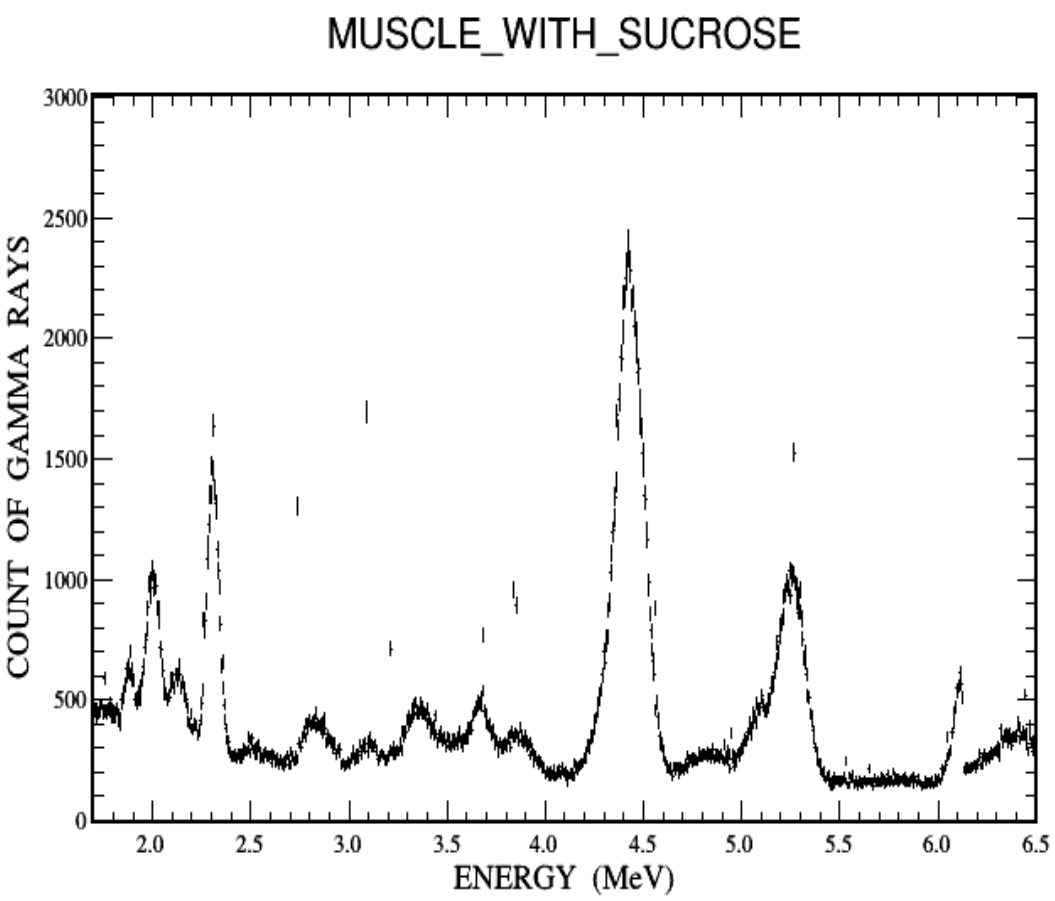

Figure 5.11 Gamma energy spectrum muscle with sucrose.

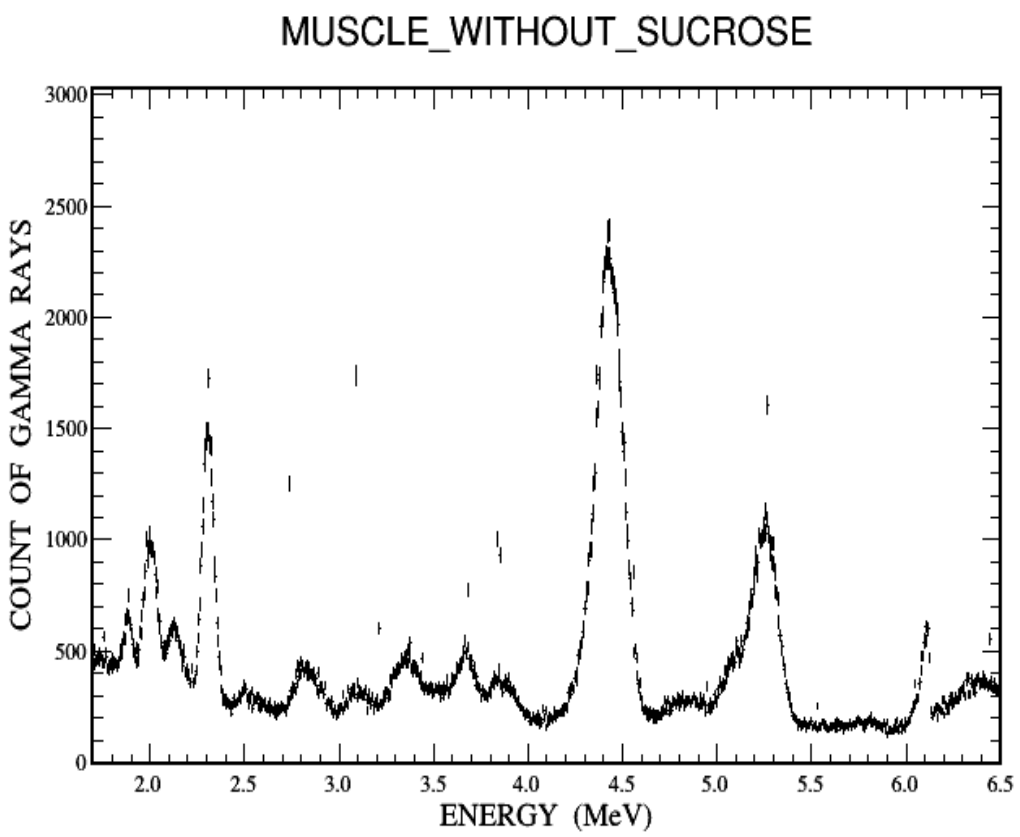

Figure 5.12 Gamma energy spectrum muscle without sucrose.

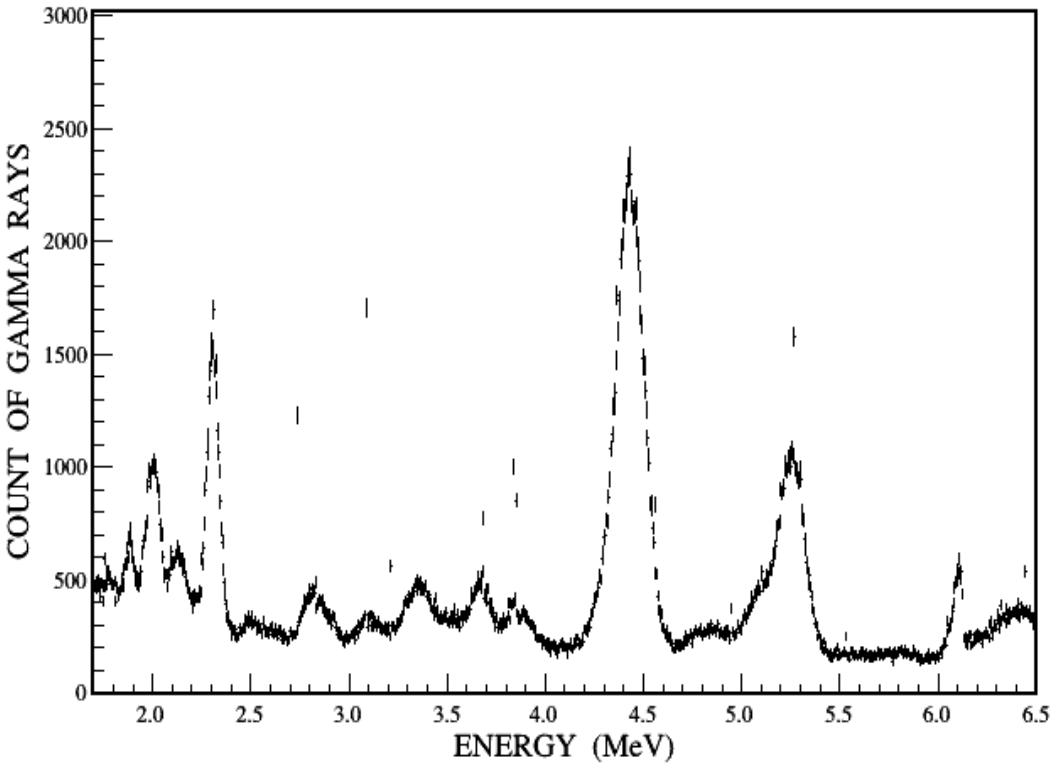

Figure 5.13 Gamma energy spectrum muscle straited.

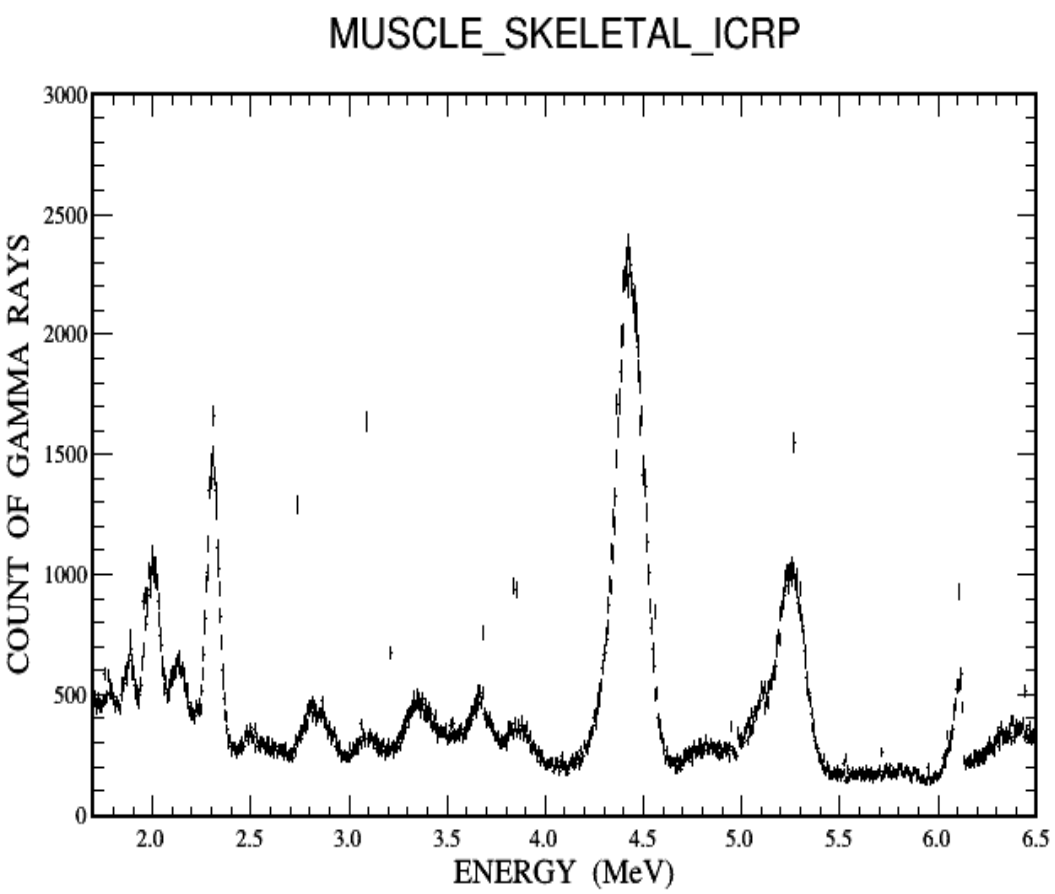

Figure 5.14 Gamma energy spectrum muscle skeletal

Each of these histograms are the result of 10,000,000 events of proton colliding with the targets. Next these spectra were compared on a peak-by-peak basis. For this, the seven most prominent peaks of the water spectrum were characterized each as Gaussian distribution with specific maximum count, mean energy, full-width half-maximum, and resolution; these features are defined next.

5.3 ANALYSIS

The analysis consists of a comparison of the most prominent resonance peaks observed in the water spectra, these peaks lie at energies 2.0 MeV, 2.31 MeV, 2.8 MeV, 3.68 MeV, 4.44 MeV, 5.2 MeV, 6.1 MeV. Figure 5.14 shows these peaks and the background of the water spectrum.

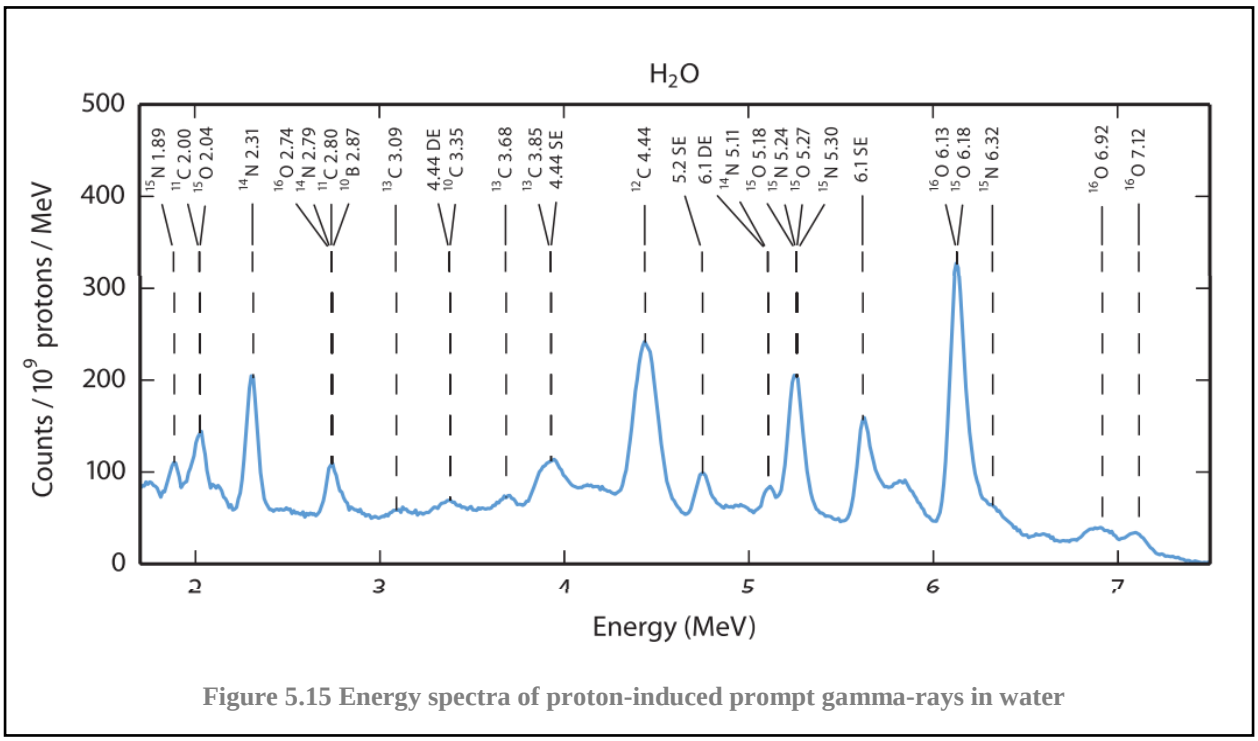

Figure 5.15 Energy spectra of proton-induced prompt gamma-rays in water

5.3.1 GAUSSIAN FIT OF PEAKS

Each of the seven peaks was analyzed by fitting the data with a Gaussian curve (also known as Normal) of the form

$$Y = \frac{1}{\sqrt{2\pi\sigma^2}} e^{-\frac{(E-E_0)^2}{2\sigma^2}}$$

Where Y is the yield or count of gammas, E_0 is the mean energy of the peak, and σ is the standard deviation (cf. Figure 5.15). The fit was performed using the software package *Origin*, and it was used to obtain their mean energy (E_0), full-width half-maximum (FWHM), maximum number of counts (Y), and peak energy resolution.

The energy resolution (R%) is the FWHM expressed as a percentage of the mean energy, R% = FWHM×100/H_0; R% is important for the design of the detector, scintillation counting equipment in nuclear medicine typically have resolutions of less than 10%.

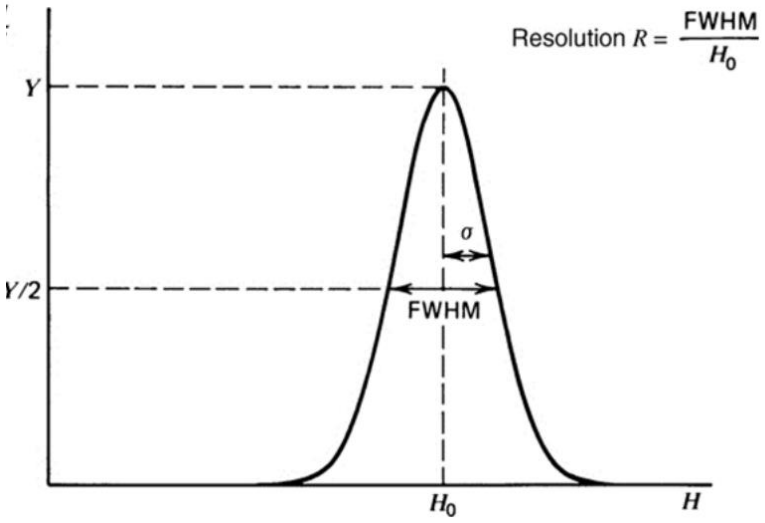

Figure 5.16 Gaussian shape used to characterize the resonant peaks

Table 5.1 shows the number of gamma rays produced in each of the seven peaks of the nine target materials at the energies 2.0 MeV, 2.31 MeV, 2.8 MeV, 3.68 MeV, 4.44 MeV, 5.2 MeV, and 6.1 MeV. The number of gamma rays were obtained by adding all of the gamma rays detected under a peak. Also listed are the gamma ray counts expressed as percentage of the water numbers.

Table 5.1 Integration peaks of body materials performed with root and normalized respect to water.

	E_0	E_0	E_0	E_0	E_0	E_0	E_0
MATERIAL	2.00 MeV	2.31 MeV	2.80 MeV	3.68 MeV	4.44 MeV	5.20 MeV	6.10 MeV
WATER	7572	12759	10500	7604	16463	8598	10177
WATER NORMALIZED (N)	100.00%	100.00%	100.00%	100.00%	100.00%	100.00%	100.00%
TISSUE	8483	12444	6568	6613	8822	8113	5438
TISSUE N	112.03%	97.53%	62.55%	86.97%	53.59%	94.36%	53.43%
BONE	20189	24968	12523	9314	19004	9906	7623
BONE N	266.63%	195.69%	119.27%	122.49%	115.43%	115.21%	74.90%
BLOOD	8132	13517	10503	7781	15812	8790	9707
BLOOD N	107.40%	105.94%	100.03%	102.33%	96.05%	102.23%	95.38%
BRAIN	8399	13431	10173	7737	15412	8670	9410
BRAIN N	110.92%	105.27%	96.89%	101.75%	93.62%	100.84%	92.46%
LUNG	8338	13299	10646	7757	15977	8806	9797
LUNG N	110.12%	104.23%	101.39%	102.01%	97.05%	102.42%	96.27%
MS20_TISSUE	11486	16675	9168	7967	13396	11478	9157
MS20_TISSUE N	151.69%	130.69%	87.31%	104.77%	81.37%	133.50%	89.98%
MUSCLE_STRIATED_ICRU	8072	12990	10081	7643	15216	8693	9507
MUSCLE_STRIATED_ICRU N	106.60%	101.81%	96.01%	100.51%	92.43%	101.10%	93.42%
MUSCLE_WITHOUT_SUCROSE	7606	12649	9997	7650	15359	8525	9379
MUSCLE_WITHOUT_SUCROSE N	100.45%	99.14%	95.21%	100.60%	93.29%	99.15%	92.16%

5.3.2 STUDY OF PEAKS

In this subsection we explain how the peaks will be characterized to allow a comparison of the resonance peaks obtained from the irradiation of different targets.

Figure 5.16 shows the gamma-ray spectrum of water and that of tissue superimposed for ease of comparison. It is easy to see that both spectra coincide in some of the resonant peaks both in energy and in maximum height (number of gammas detected), and in some others only in energy but in height, and in some do not coincide at all. For instance, at energies 2.8 MeV, 3.35 MeV, and 4.44 MeV the peaks match both in energy and height, while at 2.0 MeV, 2.31 MeV, 2.8 MeV, 3.68 MeV, 4.44 MeV and 5.2 MeV the peaks do not match in height. Taking these results at face value the peaks with a near perfect match cannot be used to distinguish between tissue and water, while

those with different height could help us distinguish between the two. To continue with the comparison of the two spectra we focus on those peaks with different heights.

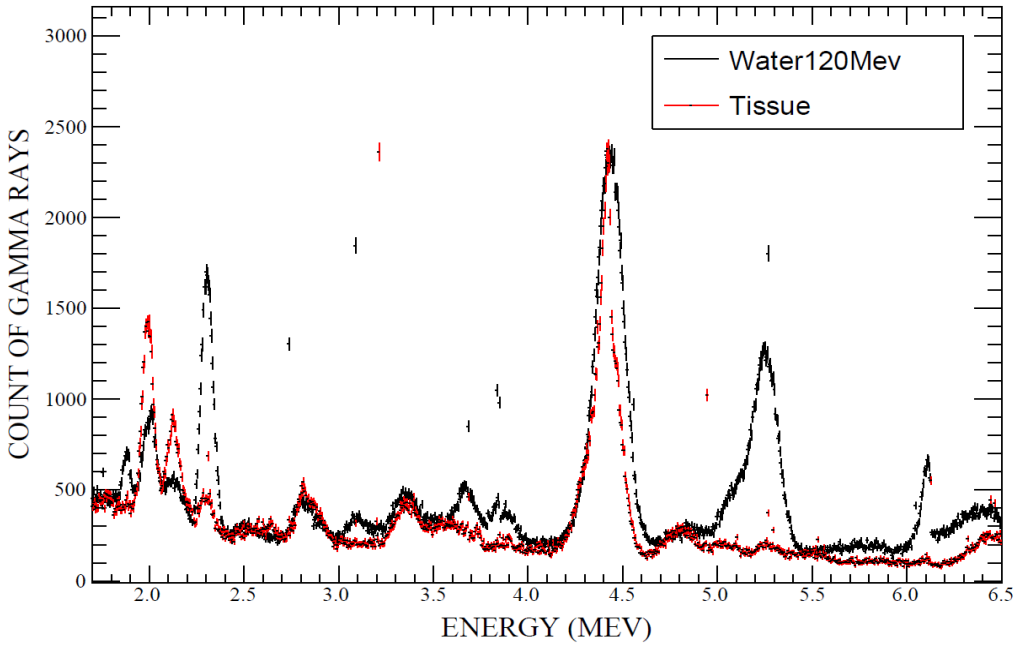

Figure 5.17 Energy spectrum of proton-induced prompt gamma-rays in water and tissue.

Figure 5.17 shows the 2.0 MeV peaks of water and tissue (solid lines) and their Gaussian fits (dashed lines). The unreadable numbers of the inset table are the parameters of the Gaussian fit, out of which the mean energy and the FWHM can be obtained, and from it the energy resolution, R, can be calculated. Figure 5.18 shows the corresponding graph for the 2.31 MeV peak.

This type of analysis will be performed for all of the peaks of interest for all of the different targets, namely muscle, lung, brain, bone, blood, Muscle with and without sucrose, striated muscle, and skeletal muscle. We will focus on extracting information (FWHM, maximum height, R and peak's area) of the seven prominent peaks of water (2, 2.31, 2.8, 3.68, 4.44, 5.2, 6.1 MeV).

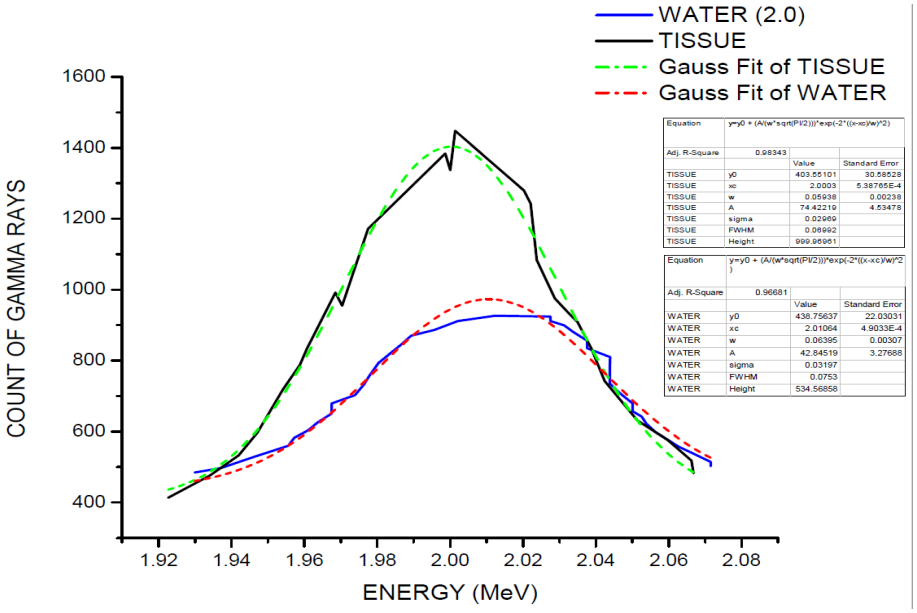

Figure 5.18 Fit of gaussian distribution in water and tissue (2.0).

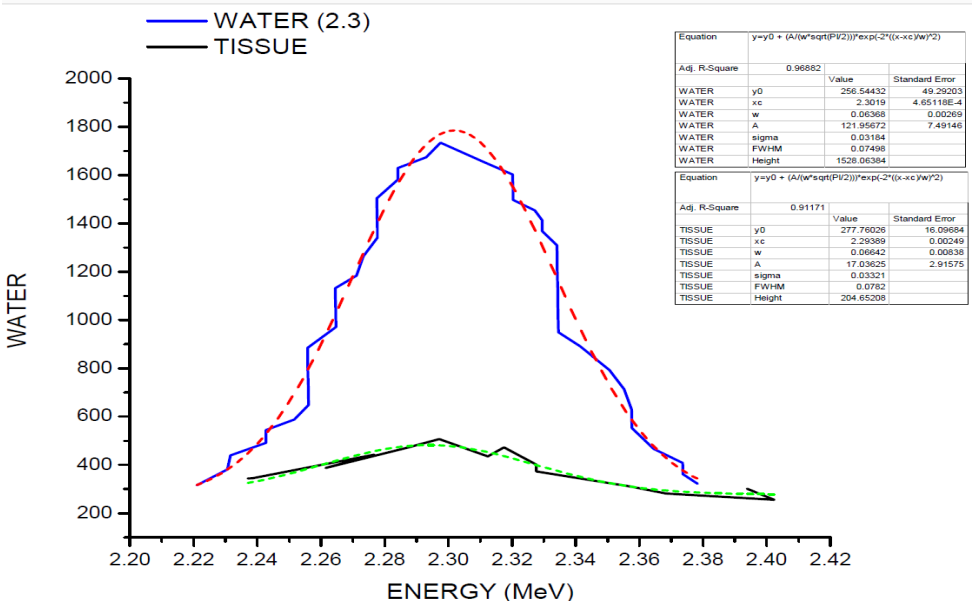

Figure 5.19 Fit of gaussian distribution in water and tissue (2.3).

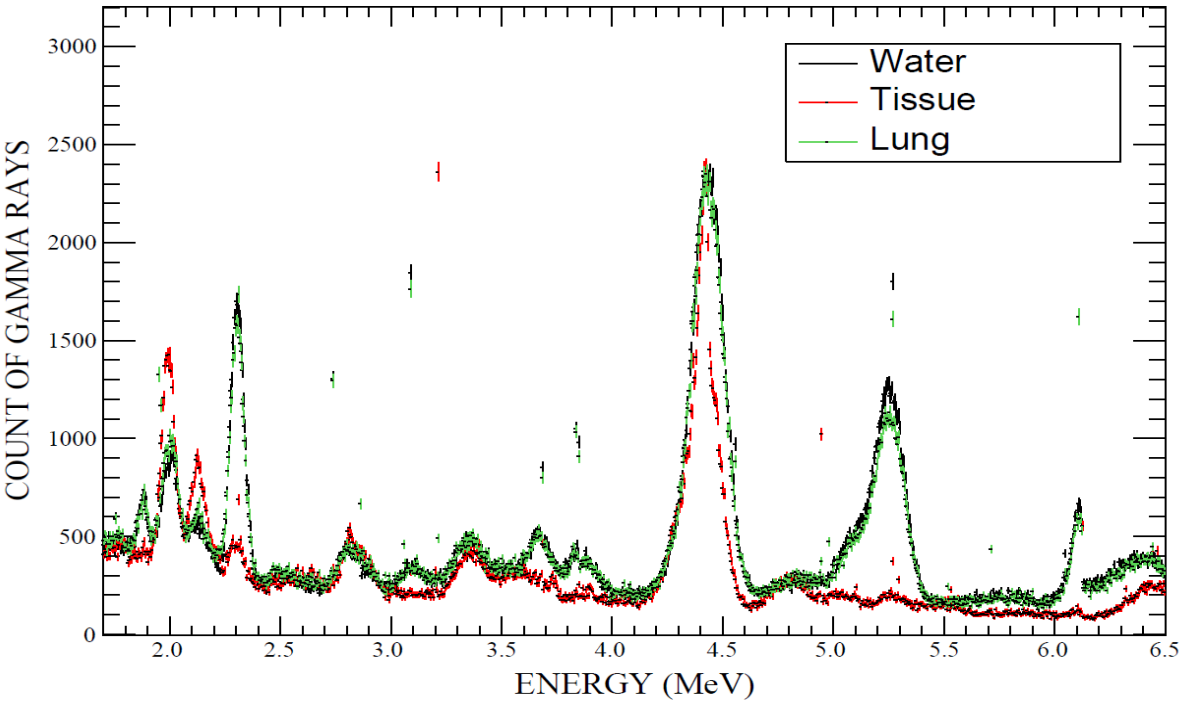

Figure 5.20 Energy spectrum of proton-induced prompt gamma-rays in water, tissue and lung.

Figure 5.19 compares the spectra of gammas produced by proton irradiation of water, tissue and lung. In this case, it is easy to see that lung is practically undistinguishable from water, and the differences with tissue are those seen before between water and tissue. Indeed, water and lung have the same FWHM and almost same intensity (a small difference of approximately 134 gamma rays).

Figure 5.20 shows the minimal differences between lung and water at the 5.2 MeV peak. Figure 5.21 compares their respective FWHM normalized to that of water of each of the peaks and Figure 5.22 does the same for the energy resolution R, which shows that at 3.68 MeV R for lung has a variation of less than 30% respect to water; similar observations can be made for the FWHM. The integration of the Gaussian shape is given by A = 1.0645×FWHM×MAXHIGH, where MAXHIGH is given by the Gaussian fit (see Figure 5.23); Figure 5.24 shows the values of A.

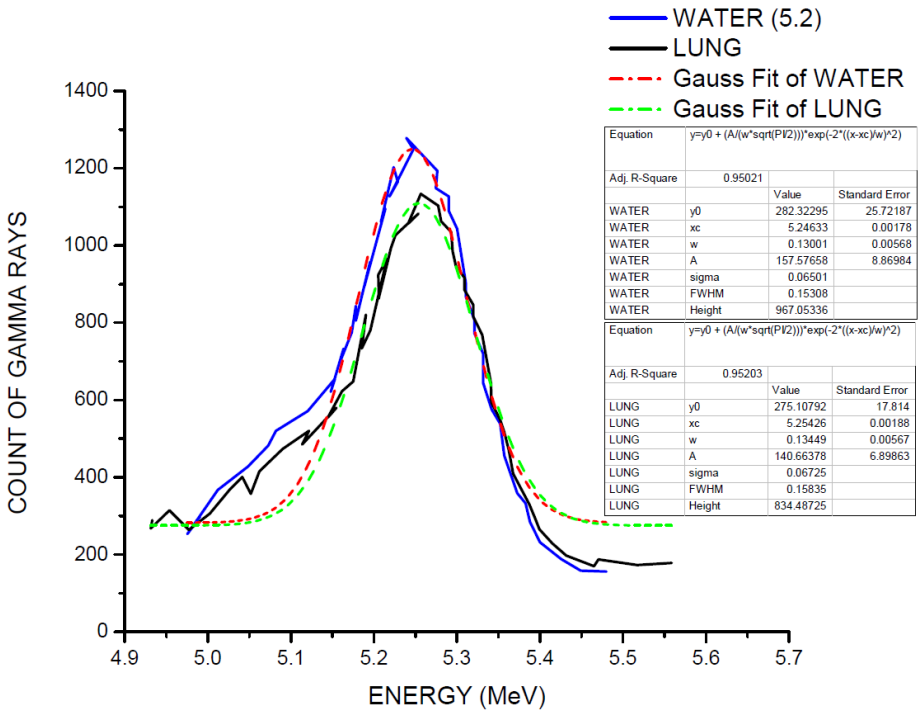

Equation	y=y0 + (A/(w*sqrt(PI/2)))*exp(-2*((x-xc)/w)^2)		
Adj. R-Square	0.95021		
		Value	Standard Error
WATER	y0	282.32295	25.72187
WATER	xc	5.24633	0.00178
WATER	w	0.13001	0.00568
WATER	A	157.57658	8.86984
WATER	sigma	0.06501	
WATER	FWHM	0.15308	
WATER	Height	967.05336	

Equation	y=y0 + (A/(w*sqrt(PI/2)))*exp(-2*((x-xc)/w)^2)		
Adj. R-Square	0.95203		
		Value	Standard Error
LUNG	y0	275.10792	17.814
LUNG	xc	5.25426	0.00188
LUNG	w	0.13449	0.00567
LUNG	A	140.66378	6.89863
LUNG	sigma	0.06725	
LUNG	FWHM	0.15835	
LUNG	Height	834.48725	

Figure 5.21 Fit of gaussian distribution in water and lung (5.2).

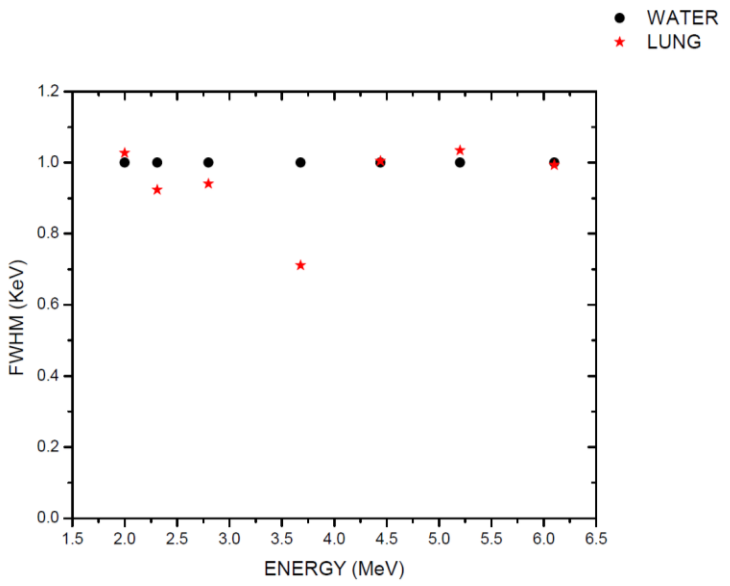

Figure 5.22 FWHM normalized of water and lung respect to water.

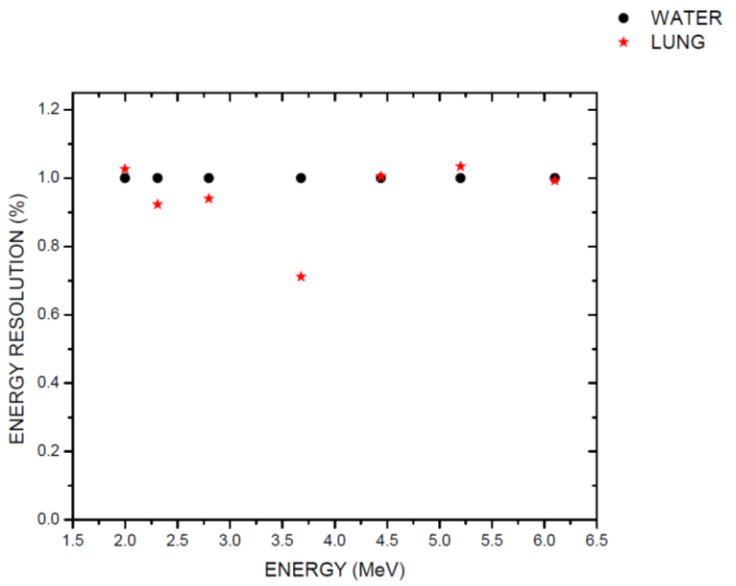

Figure 5.23 Energy resolution (r) normalized of water and lung respect to water.

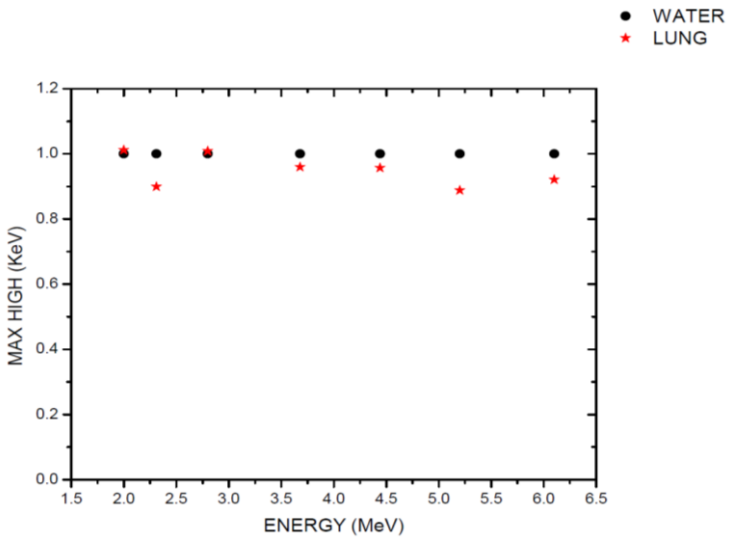

Figure 5.24 MAXHIGH normalized of water and lung respect to water.3

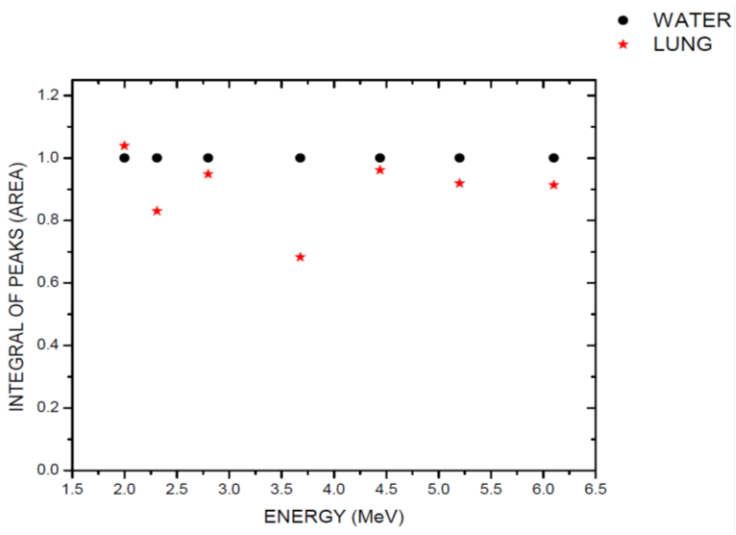

Figure 5.25 Integral of peaks normalized of water and lung respect to water.

5.3.3 RESULTS OF THE STUDY OF PEAKS

In this subsection we present all of the results obtained from the comparison of the characteristics of the resonance peaks obtained from irradiating different body parts.

Figure 5.25 show the Gaussian fit of the 5.2 MeV peak of water and tissue. Water, tissue and lung are compare to one another in terms of the FWHM (Figure 5.24), R (Figure 5.26), MAXHIGH (Figure 5.27) and integral (Figure 5.28).

Water, tissue and MS20-TISSUE are compared in Figure 5.29 (energy spectrum), FWHM (Figure 5.30), R (Figure 5.31), MAXHIGH (Figure 5.32), and integrals of peaks (Figure 5.33). The Gaussian fit of the 4.44 MeV and 5.2 MeV peaks is shown in (Figure 5.34).

Water, bone and brain are compared in Figure 5.35 (energy spectrum), FWHM (Figure 5.36), R (Figure 5.37), MAXHIGH (Figure 5.38), and integrals of peaks (Figure 5.39).

The energy spectrum of water, muscle-skeletal and muscle-striated are compared in Figure 5.40. The energy spectrum of water, muscle with sucrose and muscle without sucrose are compared in Figure 5.41. Water, muscle-skeletal and muscle-striated, muscle with sucrose and muscle without sucrose are compared in Figures 5.42 (FWHM), 5.43 (R), 5.44 (MAXHIGH), and 5.45 (peak integrals).

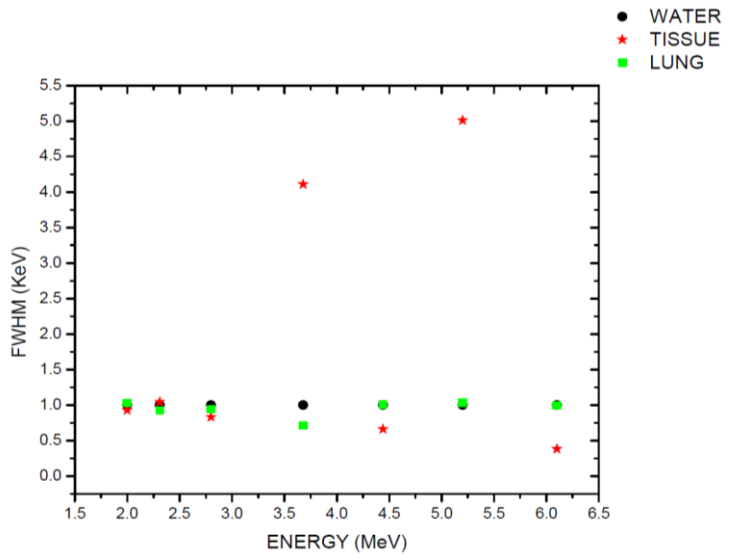

Figure 5.26 FWHM normalized of water, tissue, and lung respect to water.

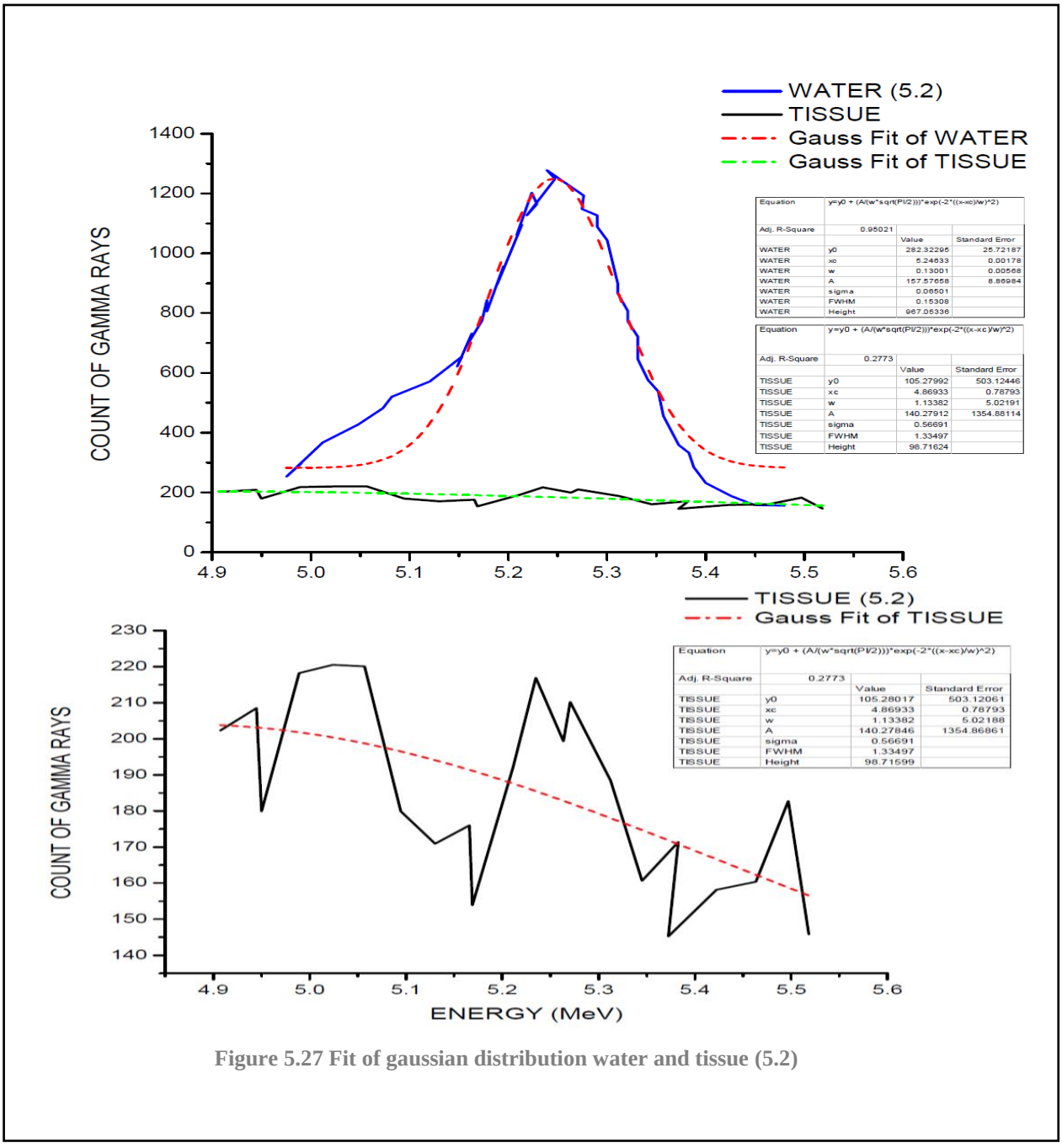

Figure 5.27 Fit of gaussian distribution water and tissue (5.2)

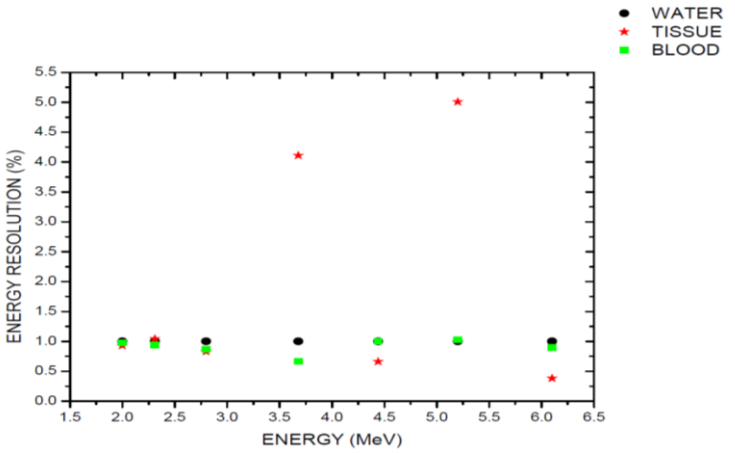

Figure 5.28 Energy resolution (r) normalized of water, tissue, and lung respect to water.

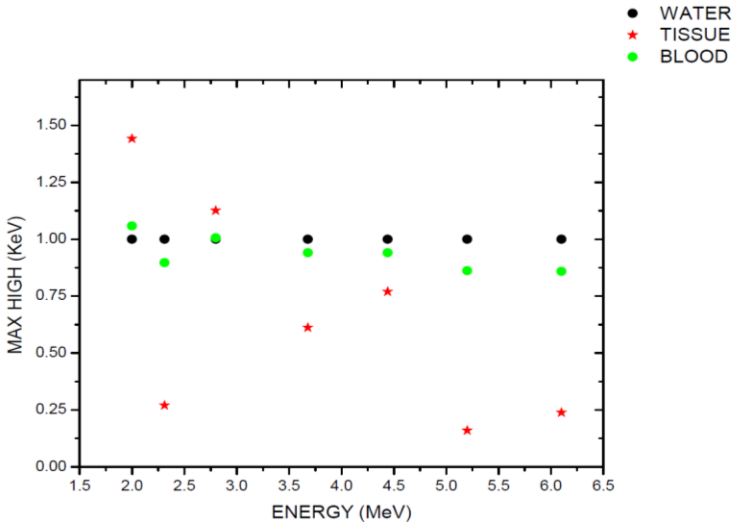

Figure 5.29 MAXHIGH normalized of water, tissue, and lung respect to water.

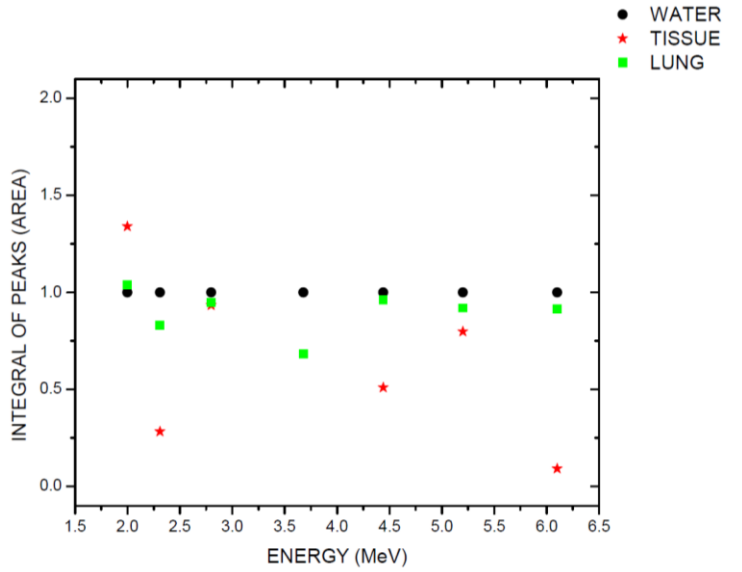

Figure 5.30 Integral of peaks normalized of water, tissue, and lung respect to water.

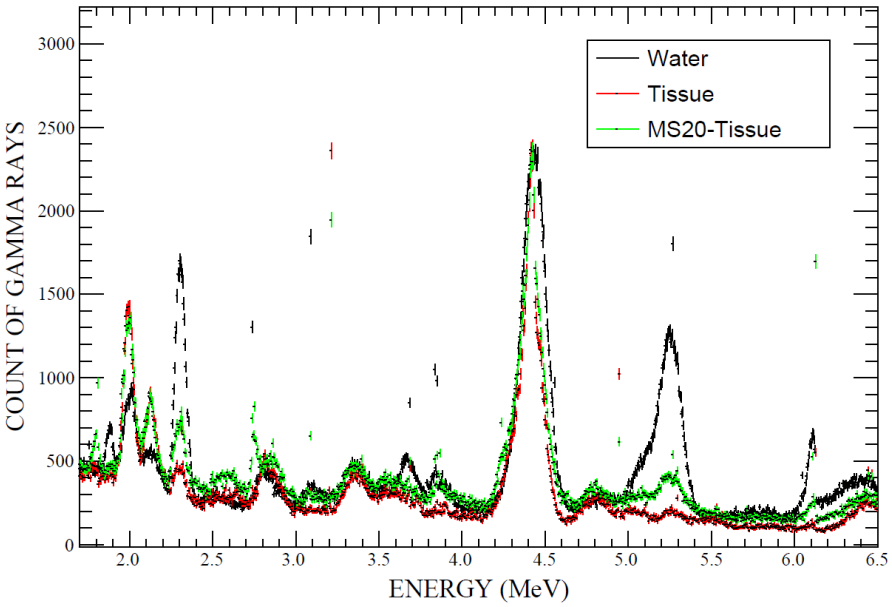

Figure 5.31 Energy spectrum of proton-induced prompt gamma-rays in water, tissue, and ms20-tissue

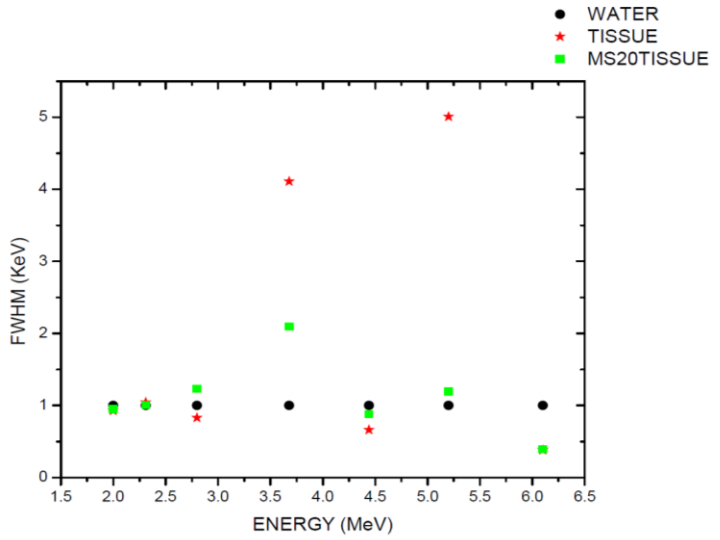

Figure 5.32 FWHM normalized of water, tissue, and ms20-tissue respect to water.

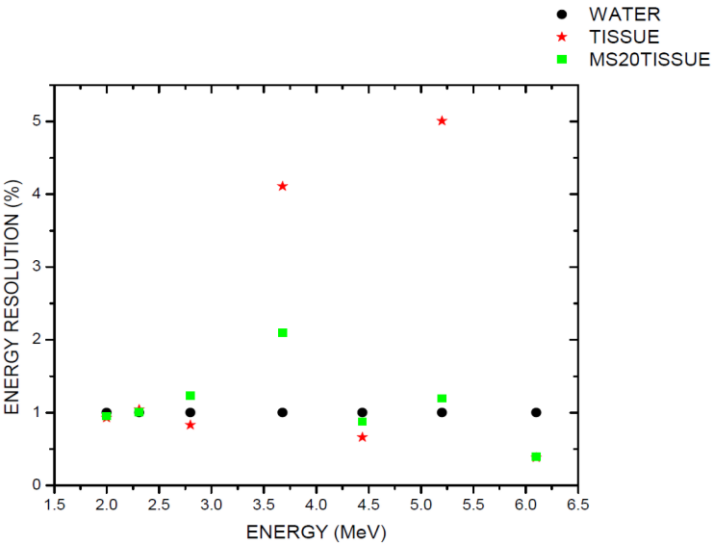

Figure 5.33 Energy resolution (r) normalized of water, tissue, and ms20-tissue respect to water.

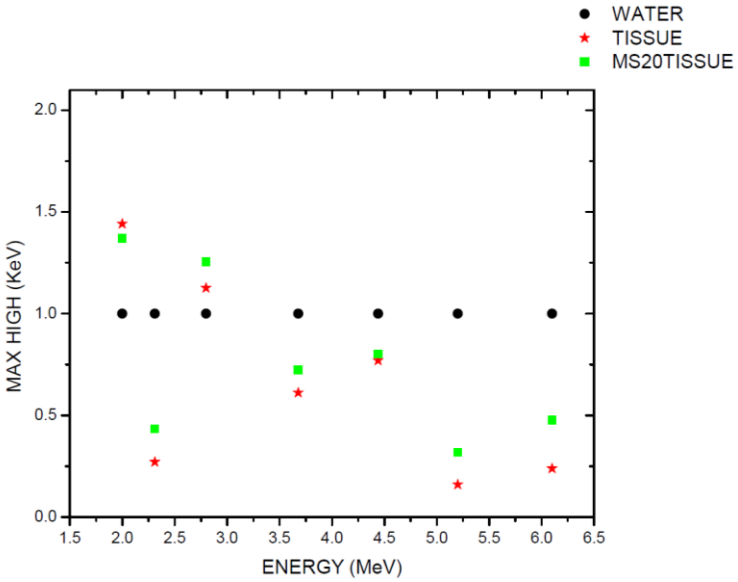

Figure 5.34 MAXHIGH normalized of water, tissue, and ms20-tissue respect to water.

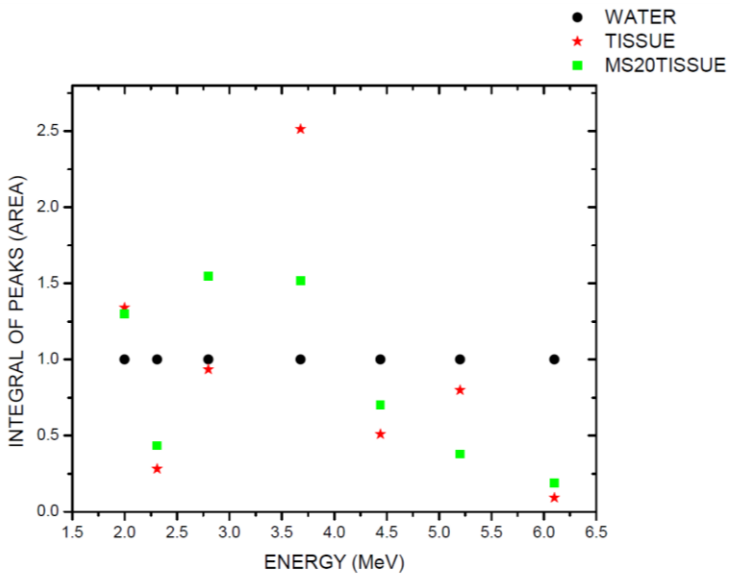

Figure 5.35 Integral of peaks normalized of water, tissue, and ms20-tissue respect to water.

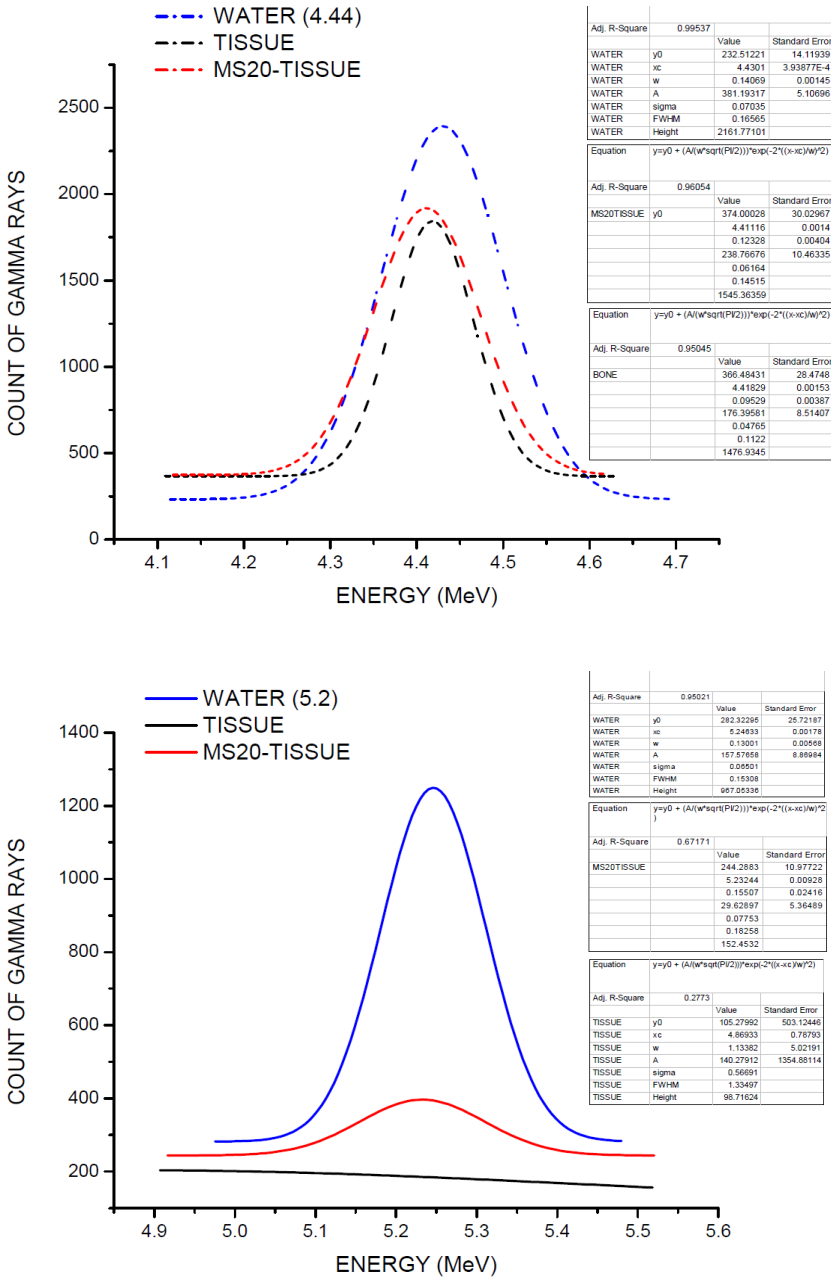

Figure 5.36 Fit of gaussian distribution of water, tissue, and ms20-tissue in 4.44 MeV and 5.2 MeV.

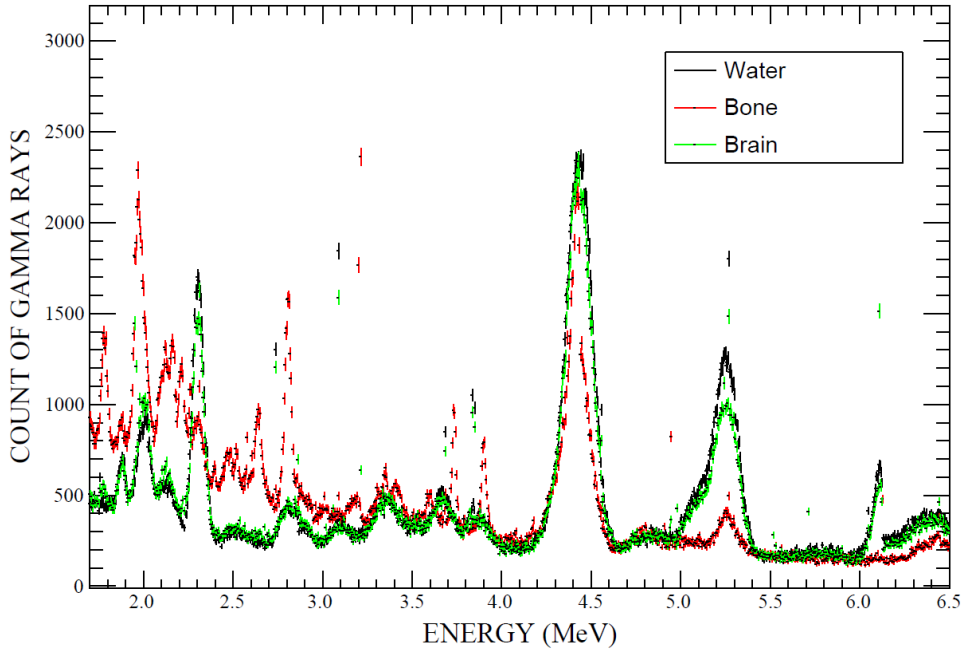

Figure 5.37 Energy spectrum of proton-induced prompt gamma-rays in water, bone, and brain.

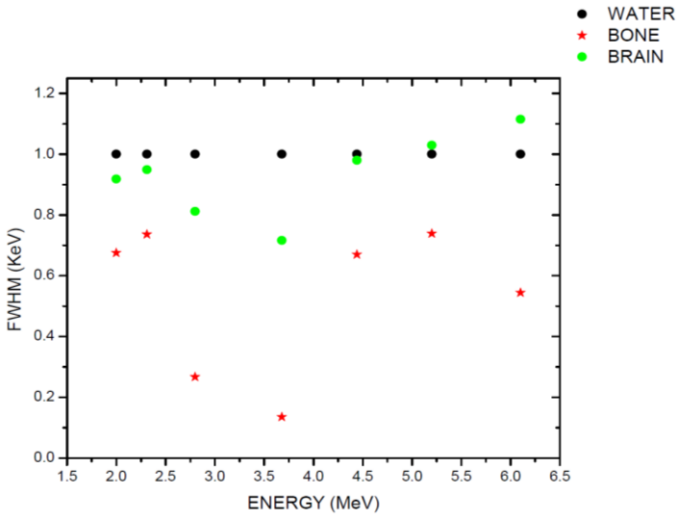

Figure 5.38 FWHM normalized of water, bone, and brain respect to water.

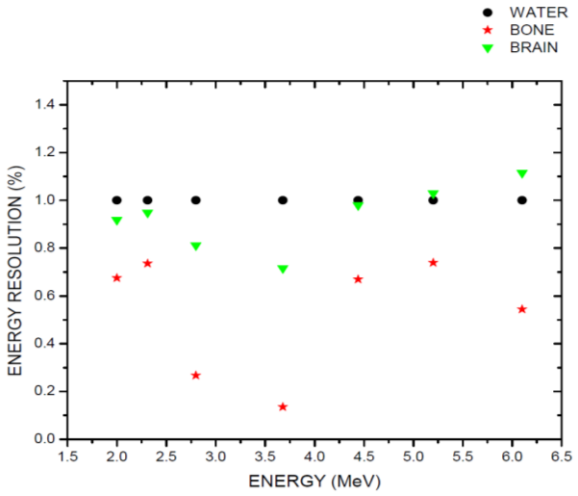

Figure 5.39 Energy resolution (r) normalized of water, bone, and brain respect to water.

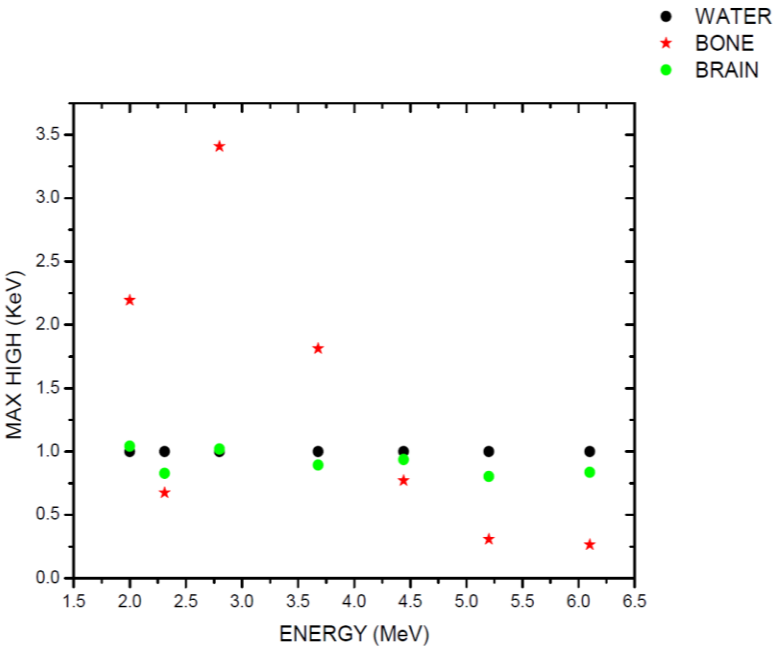

Figure 5.40 MAXHIGH normalized of water, bone, and brain respect to water.

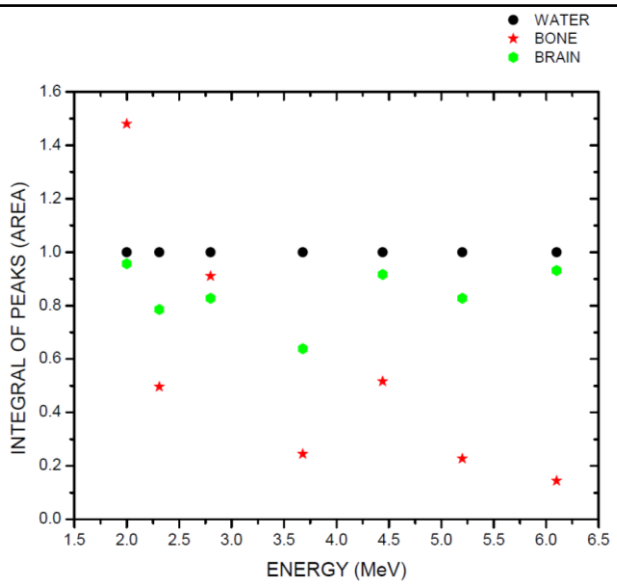

Figure 5.41 Integral of peaks normalized of water, bone, and brain to water.

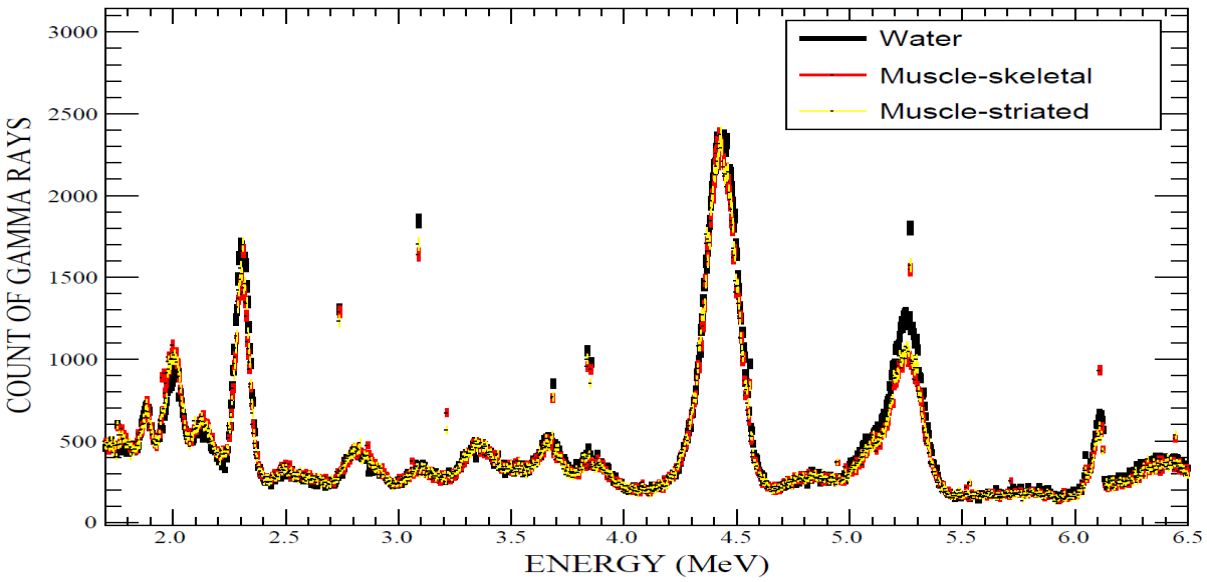

Figure 5.42 Energy spectrum of proton-induced prompt gamma-rays in water, muscle-skeletal and muscle-striated.

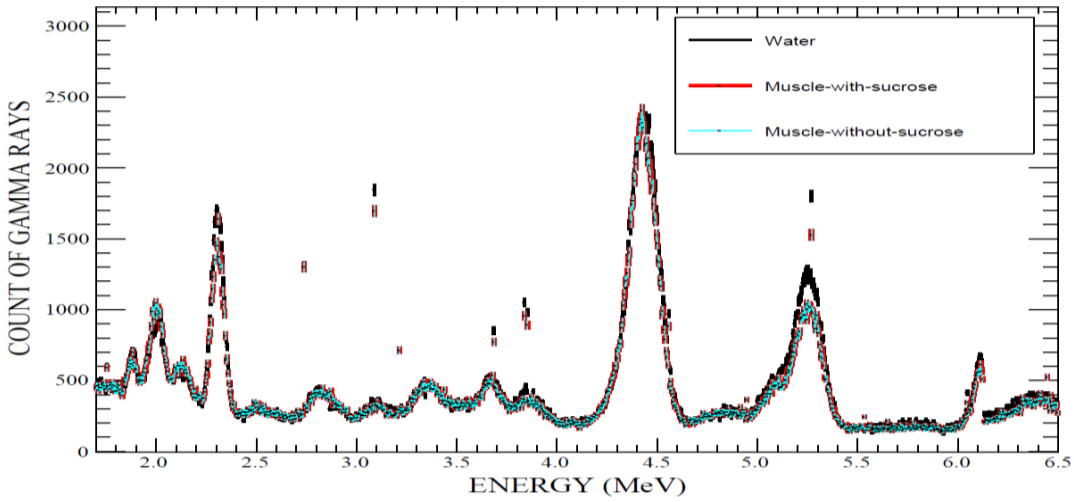

Figure 5.43 Energy spectrum of proton-induced prompt gamma-rays in water, muscle with sucrose and muscle without sucrose.

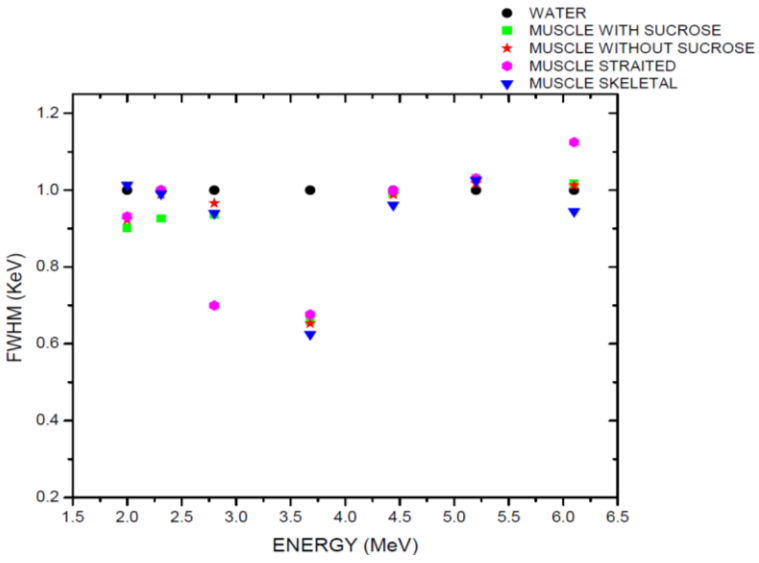

Figure 5.44 FWHM normalized of water and lung respect to water, muscle with sucrose, muscle without sucrose, muscle-striated and muscle-skeletal respect to water.

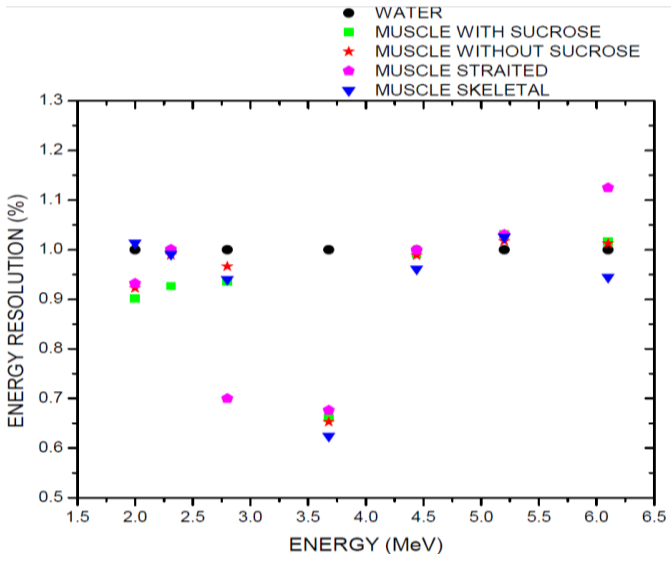

Figure 5.45 Energy resolution ® normalized of water, muscle with sucrose, muscle without sucrose, muscle-straited and muscle-skeletal respect to water.

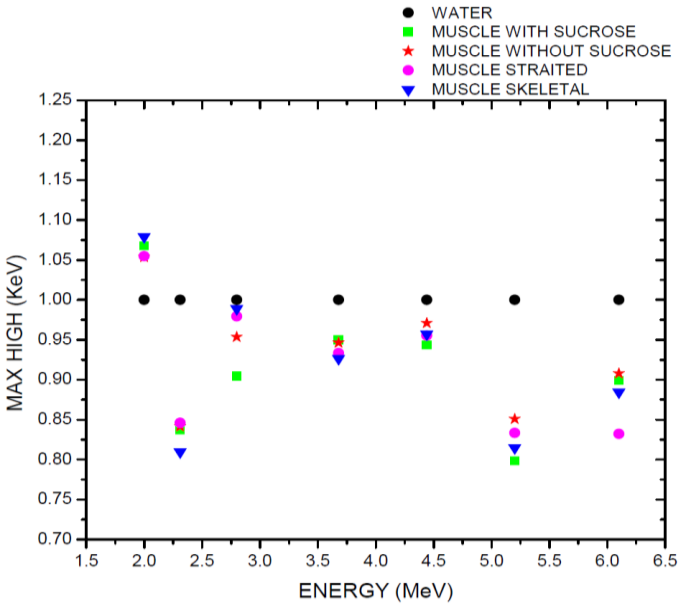

Figure 5.46 MAXHIGH normalized of water, muscle with sucrose, muscle without sucrose, muscle-straited and muscle-skeletal respect to water.

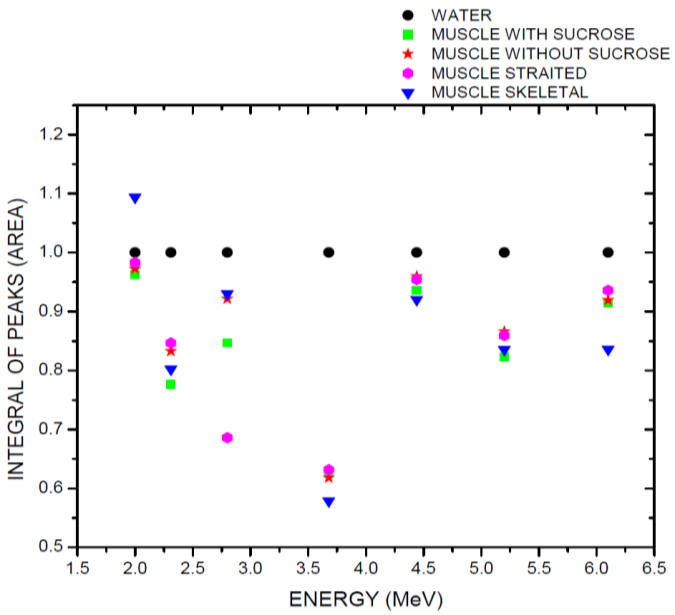

Figure 5.47 Integral of peaks normalized of water, muscle with sucrose, muscle without sucrose, muscle-straited and muscle-skeletal respect to water.

5.3.4 OBSERVATIONS OF THE STUDY OF PEAKS

To be able to summarize the results and reach some conclusions it is convenient to make a list of some interesting features observed in the previous figures. Without any particular hierarchy we present them as bullets.

- For the peak at 3.68 MeV the lung's integral (A) it is less than water's A by 30%, and for the peak at 2.3 MeV the difference is around 15%. These two points are promising signatures to distinguish between lung and water.
- For the peak at 3.68 MeV the tissue's FWHM is bigger than water's by more than 300%, and for the 5.2 MeV peak is around 400% greater. This happens because the lung spectrum does not show strong peaks in these two energies.

- Figure 5.27 indicates there is a pronounced difference in the values of MAXHIGH for blood and water or tissue and, thus, it is possible to distinguish between these two materials at some energies.
- Figure 5.28 shows that tissue has different integral values (A) than water or lung at the 2 MeV peak of 30%, approximately, at 2.3 MeV of 75%, and at 3.68 MeV of about 150%.
- Water, tissue and MS20-tissue have like spectra but at the energy of 3.68 MeV muscle (of any kind) yields way less gammas than water.
- R for water, tissue and MS20-tissue (Figure 5.31) present a major difference at 3.68 MeV where R for MS20-tissue it is greater by 100% than water. We suspect this to be true due to the fact that tissue nor MS20-Tissue do not present a peak at such energy.
- Figure 5.32 shows a similar effect for FWHM at 2 MeV, namely MS20-tissue and normal tissue differ from water by about 50% in the same energy.
- In Figure 5.33 in the energies 3.68 MeV and 5.2 MeV the values for (R) for tissue are very huge compare with water and MS20-tissue by 400% more in both cases because the FWHM was applied incorrect.
- In Figure 5.34 it is observed that tissue and MS20-tissue almost match together in each energy.
- Figure 5.35 the integral for the energy 3.68 MeV for tissue is 150% greater than water and for MS20-tissue is 50% greater than water.
- In Figure 5.36 there are two gausses fit in the energy 4.44 MeV where it can be observed that tissue and MS20-tissue are very similar. However, in the energy 5.2 MeV there is a complete difference between these two materials.
- In Figure 5.37 there is a gamma spectrum of three materials: water, bone, and brain. It can be observed that bone has a very different spectra respect the spectra of water and brain.

- In Figure 5.38 the FWHM of brain is very similar, but in the energies 2.8 MeV and 3.68 MeV there is a considerable difference. Now, respect the bone material, there is a huge difference for all the energies.
- In Figure 5.39 the energy resolution is very different for bone in all the energies and brain has a similar energy resolution compared with water.
- In figure 5.40 MAXHIGH for brain and water is very similar in all the energies. However, comparing water and bone in the energy 2.8 MeV there is a difference of 250% approximately, in energy 2.0 MeV there is a difference of 130% respect water.
- In Figure 5.41 the integral for brain is very similar to water. However, in the energy 3.68 MeV there is a considerable difference of 50% between water and brain. For bone, the integral values of (A) are different except in the energy 2.8 MeV where there is a difference of 20% between water and bone.
- In Figure 5.42 and 5.43 there are representation of gamma-rays spectra of water and 4 different kind of muscles. It can be observed that these muscles almost match identical respect water.
- In Figure 5.44 it is observed that these muscles are very similar in the FWHM. However, the muscle-straited has a difference of 30% in the energy 2.8 MeV compared with water. In the energy 3.68 MeV there is a difference of 35% approximately between water and all the muscles.
- In Figure 5.45 the values for energy resolution are very similar compared with water except for muscle-straited in the energy 2.8 respect to water with a difference of 30% approximately.
- In Figure 5.46 all the values for the muscles are identical with some difference respect to water for all the muscles.

- In figure 5.47 the values for integral (A) are very similar. However, there is a difference of 40% between all the muscles and water in the energy of 3.68 MeV.

CHAPTER 6: CONCLUSIONS

To be able to summarize the conclusions, it is convenient to make a list of some interesting features observed in the previous analysis. Without any particular hierarchy we present them as bullets.

- There are notable differences between some body materials respect gamma-ray spectra.
- Lungs, blood, and brain are very similar to the water gamma ray spectra.
- There are notable differences in tissue gamma ray spectra and bone gamma ray spectra with respect to water gamma ray spectra.
- There are not notable differences between water and all the muscles.
- There is not notable difference between tissue and MS20-tissue. However, there is an important difference in the energy 5.2 MeV.
- Tissue and water have an important difference in the energies 4.44 MeV, 5.2 MeV, and 6.1 MeV.
- It was obtained a list of data for the construction of gamma-ray detectors in the Table 6.1a and Table 6.1b.
- With all the data collected it is necessary to continue with the development of gamma ray detectors in Arizona State University.
- Find data about new variables such as gamma-ray detector sensitivity, detector efficiency, etc.
- In my personal point of view, it is necessary to continue with this research adding more data for the construction of the gamma-ray sensors enhancing the Proton Therapy.

Table 6.1a Data of body materials composed by FWHM, R%, MAXHIGH, and A.

	Xc (ENERGIES, KeV)	FWHM (KeV)	R%	MAX HIGH	INTEGRATION OF PEAKS
WATER	2000	75.3	3.765	973.21	78009.44799
	2310	74.98	3.245887	1784.6	142440.0084
	2800	160.42	5.729286	453.01	77359.19944
	3680	118.11	3.209511	541.94	68137.0838
	4440	165.65	3.730856	2394.25	422188.6971
	5200	153.08	2.943846	1249.27	203573.1188
	6200	63.89	1.030484	638.29	43410.68055
	Xc (ENERGIES, KeV)	FWHM (KeV)	R%	MAX HIGH	INTEGRATION OF PEAKS
TISSUE	2000	69.92	3.496	1403.39	104454.0932
	2310	78.2	3.385281	482.41	40157.6898
	2800	NA	NA	510	NA
	3680	NA	NA	331.46	NA
	4440	109.65	2.469595	1843.41	215167.2855
	5200	NA	NA	199.06	NA
	6200	24.37	0.393065	152.57	3957.950343
	Xc (ENERGIES, KeV)	FWHM (KeV)	R%	MAX HIGH	INTEGRATION OF PEAKS
LUNG	2000	77.33	3.8665	984.83	81069.0242
	2310	69.22	2.996537	1604.75	118245.5063
	2800	NA	NA	456.83	NA
	3680	84.01	2.28288	520.12	46513.62684
	4440	166.43	3.748423	2290.39	405776.3374
	5200	158.35	3.045192	1109.59	187036.4572
	6200	63.42	1.022903	587.55	39665.84715
	Xc (ENERGIES, KeV)	FWHM (KeV)	R%	MAX HIGH	INTEGRATION OF PEAKS
BRAIN	2000	69.13	3.4565	1013.94	74614.71406
	2310	71.13	3.079221	1478.34	111936.7781
	2800	130.23	4.651071	461.76	64013.71261
	3680	84.55	2.297554	483.38	43505.87975
	4440	162.24	3.654054	2240.09	386873.5786
	5200	157.6	3.030769	1004.05	168444.6491
	6200	71.22	1.14871	533.56	40451.15244
	Xc (ENERGIES, KeV)	FWHM (KeV)	R%	MAX HIGH	INTEGRATION OF PEAKS
BONE	2000	50.85	2.5425	2133.85	115504.9271
	2310	55.19	2.389177	1203.1	70681.83024
	2800	42.87	1.531071	1544.02	70461.53026
	3680	15.98	0.434239	981.73	16699.92433
	4440	110.92	2.498198	1846.09	217975.8583
	5200	113.08	2.174615	384.52	46286.07974
	6200	34.78	0.560968	169.11	6261.011954
	Xc (ENERGIES, KeV)	FWHM (KeV)	R%	MAX HIGH	INTEGRATION OF PEAKS
BLOOD	2000	73.6	3.68	1030.22	80714.85238
	2310	70.36	3.045887	1600.25	119855.8766
	2800	138.55	4.948214	455.79	67222.86044
	3680	78.78	2.140761	509.82	42754.17306
	4440	165.59	3.729505	2252.65	397075.8657
	5200	157	3.019231	1075.85	179803.045
	6200	57.24	0.923226	548.33	33410.83259

Table 6.1b Data of body materials composed by FWHM, R%, MAXHIGH, and A.

	Xc (ENERGIES, KeV)	FWHM (KeV)	R%	MAX HIGH	INTEGRATION OF PEAKS
MS20-TISSUE	2000	71.41	3.5705	1332.95	101325.4539
	2310	75.14	3.252814	772.79	61812.79052
	2800	197.66	7.059286	568.16	119546.0172
	3680	247.54	6.72663	392.38	103394.6138
	4440	145.15	3.269144	1919.02	296511.9541
	5200	182.58	3.511154	396.75	77110.90567
	6200	25.21	0.406613	303.85	8154.132273
	Xc (ENERGIES, KeV)	FWHM (KeV)	R%	MAX HIGH	INTEGRATION OF PEAKS
MUSCLE	2000	67.89	3.3945	1039.13	75096.78725
WITH	2310	69.48	3.007792	1494.51	110536.1416
SUCROSE	2800	150.12	5.361429	409.84	65493.55496
	3680	77.97	2.11875	514.6	42711.31885
	4440	164.28	3.7	2259.36	395107.9749
	5200	157.81	3.034808	997.21	167520.0564
	6200	64.95	1.047581	573.86	39676.26435
	Xc (ENERGIES, KeV)	FWHM (KeV)	R%	MAX HIGH	INTEGRATION OF PEAKS
MUSCLE	2000	69.48	3.474	1025.42	75841.56031
WITHOUT	2310	74.16	3.21039	1501.96	118569.7089
SUCROSE	2800	155.01	5.536071	432.01	71285.16872
	3680	77.14	2.096196	512.92	42118.69765
	4440	163.72	3.687387	2324.83	405171.2329
	5200	155.73	2.994808	1062.98	176215.0684
	6200	64.69	1.043387	579.45	39902.37852
	Xc (ENERGIES, KeV)	FWHM (KeV)	R%	MAX HIGH	INTEGRATION OF PEAKS
MUSCLE	2000	70.18	3.509	1026.48	76684.84103
STRAITED	2310	75.02	3.247619	1509.63	120557.2251
	2800	112.34	4.012143	443.67	53056.68956
	3680	79.91	2.171467	505.84	43028.8724
	4440	165.52	3.727928	2286.98	402956.8196
	5200	157.83	3.035192	1041.08	174911.8872
	6200	71.86	1.159032	531.11	40627.24352
	Xc (ENERGIES, KeV)	FWHM (KeV)	R%	MAX HIGH	INTEGRATION OF PEAKS
MUSCLE	2000	76.34	3.817	1050.16	85340.12873
SKELETAL	2310	74.31	3.216883	1444.65	114276.1417
	2800	150.86	5.387857	448.07	71955.77189
	3680	73.78	2.004891	502.06	39431.19495
	4440	159.24	3.586486	2291.96	388512.3857
	5200	156.99	3.019038	1017.89	170105.5576
	6200	60.37	0.97371	564.57	36281.45026

REFERENCES

[AAPM, 2018] American Association of Physics in Medicine. Retrieved on 2018-1-31 from https://www.aapm.org/publicgeneral/.

[Camphausen, 2008] Camphausen, K. A.; Lawrence, R. C. (2008). "Principles of Radiation Therapy". In Pazdur, R.; Wagman, L. D.; metzLevin, K. A.; Hoskins, W. J. (eds.) Cancer Management: A Multidisciplinary Approach. 11th ed.

[European Science Foundation, 2010]. Perspectives of Nuclear Physics in Europe.

[Fix, 2013] Macro Monte Carlo for dose calculation of proton beams, Michael K Fix, Phys. Med. Biol. 58 (2013) 2027.

[Geant4, 2018] Geant4 official website, Retrieved on 2018-2-1 from http://geant4.cern.ch/support/introductionToGeant4.shtml.

[Holmes, 2017] Physics seminar at UTEP, 2017, Jason Holmes, Arizona State, “Next generation detectors for proton therapy quality assurance”.

[Knopf, 2013] In vivo proton range verification: a review, Antje-Christin Knopf and Antony Lomax, Phys. Med. Biol. 58 (2013) R131.

[Levin, 2005] Levin, W. P.; Kooy, H.; Loeffler, J. S.; DeLaney, T. F. (2005). "Proton Beam Therapy", British Journal of Cancer 93, 849–854.

[Mayo, 2018] Mayo Foundation for Medical Education and Research (MFMER). Retrieved on 2018-1-29 from https://www.mayoclinic.org/departments-centers/mayo-clinic-cancer-center.

[Metz, 2006] Metz, James (2006-07-31). "Differences Between Protons and X-rays". Abramson Cancer Center of the University of Pennsylvania. Retrieved on 2008-02-04 from http://www.oncolink.org/treatment/article.cfm?c=9&s=70&id=210.

[NAPT, 2016] National Association for Proton Therapy, 2016, link.

[Newhauser, 2015] The physics of proton therapy, Wayne D Newhauser and Rui Zhang, Phys. Med. Biol. 60 (2015) R155–R209.

[Nuclear Physics, 2015] Long Range Plan for Nuclear Physics.

[PTCOG, 2013] "Particle therapy facilities in operation". Particle Therapy Co-Operative Group. 2013-08-27. Retrieved on 2014-09-01 from http://www.ptcog.ch/index.php/facilities-in-operation.

[ROOT, 2018] ROOT Data Analysis Framework. Retrieved on 2018-2-1 from https://root.cern.ch/.

[Wilson, 1946] "Radiological Use of Fast Protons", R. R. Wilson, Radiology, 47:487-491 (1946).

VITA

Omar Hernandez Rodriguez has the Master of Science in Physics at University of Texas at El Paso, May 2018 – present. Thesis title: “Geant4 study of protons-body interactions” and Bachelor of Engineering in Physics in Universidad Autónoma de Ciudad Juárez, May 2015.

Graduate Teaching Assistant in Department of Physics at University of Texas at El Paso, August 2016 - present. Responsibilities include: assisting professors with the preparation and presentation of undergraduate courses, grading, and tutoring. And presentation of Geant4 study of protons-body interactions.in the meeting of the American Physical Society at University of Texas at Dallas, Dallas, Texas, October 2017. Actual member of American Physical Society.

Contact Information: ohernandez21@miners.utep.edu

This thesis was typed by Omar Hernandez Rodriguez